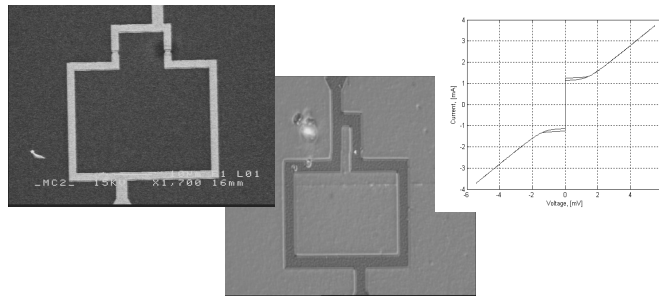


THESIS FOR THE DEGREE OF MASTER OF SCIENCE

# Feasibility study of HTS flux qubit read-out using aluminium dc-SQUID

Jesper Johansson



**CHALMERS**

Department of Microtechnology and nanoscience,  
Quantum Device Physics Laboratory  
Chalmers University of Technology  
Göteborg, Sweden

Supervisors: Dr. Serge Charlebois, University of Sherbrooke,  
M.Sc. Tobias Lindström, CTH

Examiner: Prof. Tord Claeson, CTH

Göteborg, November 2003

**Front cover illustration:** (top left) SEM image of an aluminium SQUID, (middle), Optical micrograph of an YBCO SQUID with grain boundary junctions, (right), I-V characteristics of a YBCO SQUID.

# Preface

During my time as a Master student at Chalmers University of Technology, (Civilingenjör, teknisk fysik) most phenomena presented in the courses were described by a Quantum Mechanical approach. However, in text books all problems were treating microscopic systems, such as atoms and sometimes molecules. An atom is something rather abstract, something that you never have the opportunity to see with your eyes. The meaning and the importance of the quantum mechanics is somewhat rubbed out in such examples. One might ask oneself: "How large may a system be in order to favor a quantum mechanical description?" Could it be something macroscopic, visible? As a matter of fact the answer is yes.

When a superconductor is cooled below its critical temperature, the electrons form pairs, known as Cooper pairs. Furthermore, all the Cooper pairs are condensed into the lowest energy level. As a consequence they all have the same wavefunction. Devices made out of superconductors may be several tenths of microns large and still enable a simple quantum mechanical description of them. Devices of this size are surely visible. They are not something abstract as atoms.

Research in the field of superconductivity has been going on the since several decades at Chalmers University of Technology. Tunnelling experiments on superconductors begun in the mid sixties. There is competence available in the field of low- $T_c$  superconductivity and low- $T_c$  devices as well as in the field of high- $T_c$  superconductivity and high- $T_c$  devices in the Quantum Device Laboratory group. Furthermore the process laboratory at MC2 provides excellent conditions for fabrication of micron- and nano sized devices. Thus, the opportunities for realizing a macroscopic quantum mechanical system are very good here.



# Abstract

This thesis for the degree of Master of Science studies and tests the feasibility of HTS flux qubit read-out using an aluminium dc-SQUID. The feasibility is studied on a device consisting of an YBCO dc-SQUID surrounded by an aluminium dc-SQUID separated by an intermediate layer. The intermediate layer acts as insulator between the YBCO and the aluminium and as capping layer for the underlying YBCO. Each part of the device has been studied within this project.

Aluminium dc-SQUIDS for flux qubit read-out have been fabricated using electron beam lithography and shadow evaporation. A typical SQUID had a critical current of 56 nA and was highly under-damped. The SQUIDS were characterized below 300 mK. An intermediate layer consisting of amorphous STO, deposited at room temperature, and thermally evaporated silicon dioxide has been studied. The roughness, peak-to-valley, was found to be approximately 10 nm and the resistance was 9 k $\Omega$  for an 360 nm thick layer of silicon dioxide and 12 k $\Omega$  for a 500 nm thick layer at 4.2 K. YBCO SQUIDS were fabricated on STO 0 $^\circ$ /30 $^\circ$  bi-crystals using electron beam lithography and ion milling through a mask of amorphous carbon. The properties of the grain boundary junctions in the SQUIDS were unchanged when a multi-layer of amorphous STO and silicon dioxide was deposited on top of them. A SQUID that consists of 3  $\mu$ m wide junctions typically had a critical current of 1.5 mA. It was found that the insulating properties, the adhesion and the smoothness of the intermediate layer has to be improved in order to get the proposed device working.



# Acknowledgements

First, I would like to thank my supervisors during this project, Serge Charlebois and Tobias Linström. Serge for teaching and coaching me in the cleanroom and for many good ideas regarding design of devices and the setup. Tobias for the help during the measurements and with interpretation of the data.

Second, I would like to thank Tord Claeson, the examiner of this thesis, for sharing valuable experience and for emphasizing the importance of limitations in a diploma work.

I would also like to thank Floriana Lombardi for helping me with questions and issues regarding fabrication of HTS devices during the fall 2003. Many thanks to Khaled Khamchane for film deposition and characterization, Jessica Gauthier and Robert Gunnarsson for helping me with the AFM and all other peoples in the QDP group.

Finally I would like to thank my parents for their support during my time as a student at Chalmers.

Göteborg, November 2003

J.J.



# Contents

<b>Preface</b>	<b>iii</b>
<b>Abstract</b>	<b>v</b>
<b>Acknowledgements</b>	<b>vii</b>
<b>Contents</b>	<b>x</b>
<b>1 General Introduction</b>	<b>1</b>
1.1 Flux Qubits . . . . .	2
1.2 Dc-SQUIDs for flux qubit readout . . . . .	3
<b>2 Motivation</b>	<b>5</b>
2.1 Aim and Objective . . . . .	6
2.1.1 Step I. Fabrication and characterization of aluminum SQUIDs . . . . .	6
2.1.2 Step II. Study of insulating and capping materials . . . . .	7
2.1.3 Step III. Read-out of an YBCO SQUID using a surrounding aluminium SQUID . . . . .	8
<b>3 Theoretical introduction</b>	<b>9</b>
3.1 DC Josephson effect . . . . .	10
3.2 AC Josephson effect . . . . .	11
3.3 Superconducting QUantum Interference Device, SQUID . . . . .	15
3.4 Electrical Insulation and Capping of YBCO . . . . .	17
3.4.1 Capping of YBCO . . . . .	17
3.4.2 Electrically insulating layer . . . . .	18
<b>4 Design and experiment</b>	<b>19</b>
4.1 Operation/Method . . . . .	20
4.2 Specification . . . . .	21
4.3 Aluminium SQUIDs . . . . .	22

4.3.1	Aluminium SQUID design . . . . .	23
4.4	YBCO SQUIDS . . . . .	25
4.5	Capping and Insulating layer . . . . .	25
4.5.1	Experiments . . . . .	26
4.6	Final design . . . . .	27
<b>5</b>	<b>Sample Fabrication</b>	<b>29</b>
5.1	Film Deposition and Characterization . . . . .	29
5.2	Pattern formation in YBCO films . . . . .	30
5.3	Aluminium SQUIDS . . . . .	31
5.3.1	Gold pads and Alignment marks using photolithography	31
5.3.2	Aluminium SQUID:s using E-beam lithography and shadow evaporation . . . . .	32
5.4	Deposition of Capping and Insulation layer . . . . .	33
<b>6</b>	<b>Measurement setup</b>	<b>35</b>
<b>7</b>	<b>Result and discussion</b>	<b>37</b>
7.1	YBCO SQUIDS . . . . .	37
7.2	Insulating properties of $\text{SiO}_{2-x}$ . . . . .	41
7.3	Surface morphology and adhesion of capping/insulating layer .	43
7.4	YBCO degradation . . . . .	45
7.5	Aluminium SQUIDS . . . . .	47
<b>8</b>	<b>Conclusion</b>	<b>51</b>
	<b>Bibliography</b>	<b>55</b>

# Chapter 1

## General Introduction

During the last 3 decades the number of transistors on a silicon chip have doubled every 18 months. Many researcher and engineers claim that silicon technology will hit a wall in a near future because of the physical limitations of the technology. The physical limitations connected with silicon are far from the ultimate limitations for a computer as described in [1] but may hinder the development. As a consequence great effort is nowadays put into the field of novel computer technologies. However, even if the computers of today becomes faster they have limitations. They cannot solve certain classes of problems in finite time e.g. problems of the nondeterministic polynomial complexity class, NP. A quantum computer doesn't have these limitations. It's capable of solving NP problems, such as factorization of large numbers, in finite time.

The basic building block of a quantum computer is the Quantum bit, "qubit". The difference between an ordinary bit that has two states, either '0' or '1', and a qubit is that the later can be in a state other than  $|0\rangle$  or  $|1\rangle$ .

$$|\psi\rangle = \alpha|0\rangle + \beta|1\rangle; |\alpha|^2 + |\beta|^2 = 1 \quad (1.1)$$

It is also possible to form linear combinations of states, superpositions. The wave nature of a quantum system results in a coherence of the superpositions. This coherence means that the basic processing components of a quantum computer have a common phase. A classical memory register that has  $N$  bits, each of which can be in one of the two states 0 and 1, can store any one of  $2^N$  configurations at a given time. However, a quantum register that contains  $N$  quantum bits, qubits, can store a coherent superposition of all  $2^N$  configurations at the same time. Herein lies the real power of quantum computers. The storage of information relies on quantum entanglement.

This means that the individual qubits in the  $N$  qubit states of the quantum memory are not independent. The information is actually stored in the entire quantum memory and in states that may have non-classical correlations. The power of a quantum computer is exemplified in [2]. Classically, a fast Fourier transform takes roughly  $N \log N = n2^n$  steps to Fourier transform  $N = 2^n$  numbers. On a quantum computer, the Fourier transform is accomplished using about  $\log N = n \log 2$  steps, an exponential speedup! Quantum search algorithms, such as Grover's search algorithm, usually offers quadratic speedup.

Much interest has been focused on natural qubits such as the states of electrons in atoms or the nuclear spins of molecules in liquid solution. In [3] and [4] systems with up to seven qubits have been realized using NMR technique. The Deutsch-Jozsa algorithm have been implemented using an ion-trap quantum computer in [5]. However, to create a really interesting quantum computer that contain 1000 qubits or more, solid state nanotechnology has to be used, [6].

In 1999 quantum oscillations of a "charge" qubit consisting of a small superconducting island connected to a superconducting electrode was shown for the first time, [7]. In the same year a "flux" qubit that was based on the superposition of two counter-rotating currents in a small superconducting aluminium ring was shown, [8], and in 2000 in Niobium, [9]. These developments started a race towards a proof-of-concepts for superconducting quantum information processors.

## 1.1 Flux Qubits

Superconducting materials are useful for making qubits because their behavior is governed by macroscopic quantum coherence. An artificial two level system, isolated from higher excitations, is formed by adding a periodic potential to the parabolic potential of a superconducting ring. If the potential barrier between the two wells is high then each well represents a state with left,  $|L\rangle$ , or right,  $|R\rangle$  circulating currents. By lowering the barrier the energy levels overlap and the circuit can be in one or two new physical states that are superpositions of both left- and right-rotating currents: a ground state  $|g\rangle = |L\rangle + |R\rangle$  and an excited state  $|e\rangle = |L\rangle - |R\rangle$ . To detect whether the qubit is in state  $|L\rangle$ , "0" or  $|R\rangle$ , "1" one observes it, just like opening the box in the example of Schrödinger's cat experiment.

In the Delft experiment, [8], [10] and [11] the qubit consists of a three junction loop of aluminium that is strongly coupled to a dc-SQUID. By changing the magnetic flux through the qubit loop the separation of the energy levels in the two-level system is controlled. The idea is that an external magnetic flux sets the system at the symmetry point of the potential, where it is in its ground state. A microwave pulse that is tuned to the energy separation of the levels is then switched on, which causes the system to perform Rabi-oscillations between the ground- and the excited-state. However, all this is done using low- $T_c$  material, aluminium. Similar results using a qubit made out of a high- $T_c$  superconductor, HTS, such as YBCO, where advantages of the symmetry properties of HTS grain boundary Josephson junctions, GBJJ is used, have never been published.

A simple design for a HTS flux qubit which uses the symmetry properties of HTS GBJJ is proposed in [12]. The proposed qubit does not need to be flux biased to reach its symmetry point as its low- $T_c$  counterpart, and it is stable to external perturbations to the 2:nd or 3:rd order. Feasibility studies of ultra small GBJJ intended for HTS qubits are presented in [13] and [14]. However, the problem associated with fabrication of an accurate read-out device on the same chip as the qubit is not solved.

## 1.2 Dc-SQUIDs for flux qubit readout

The states in a flux qubit are represented by the direction of the persistent Josephson currents. These currents produce a flux when circulating in the superconducting loop. DC-SQUIDs are one of the most accurate flux-to-voltage converters available. The accuracy is better than a quantum flux,  $\Phi_0$ ,  $10^{-16}$  -  $10^{-15}$  Tesla. Thus, DC-SQUIDs can distinguish between the current states in the qubit by measuring the direction of the induced flux.

DC-SQUIDs are used for flux qubit readout in, [8], [10], [11], and [15]. An under damped aluminium SQUID is used in all experiment in order to minimize the damping of the quantum system.



# Chapter 2

## Motivation

The state of a flux qubit is determined by the direction of the persistent Josephson current. We want to study whether it is possible to use an aluminium dc-SQUID as read-out device for a HTS flux qubit. A dc-SQUID can be current and flux biased so that a circulating current appears in the superconducting loop of the SQUID. Thus, a system qualitatively comparable with the flux qubit systems presented in [8], [9], [10], [11], [12] and [15] is obtained by combining two dc-SQUIDs in a concentric configuration. The biasing leads have to be isolated from each other by an intermediate layer. The intermediate multi-layer is not necessary for a flux qubit device but in this experiment it enables us to control the two SQUIDs individually.

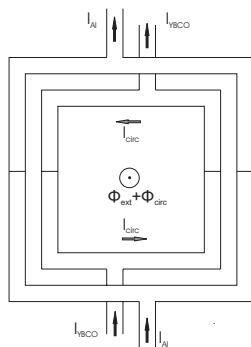


Figure 2.1: Proposed experimental setup. An aluminium dc-SQUID surrounding an YBCO dc-SQUID.

In this study a system consisting of a YBCO grain boundary dc-SQUID and an aluminium dc-SQUID is proposed, see figure 2.1. Such a system enables testing of the strength of the mutual inductance between the two devices and the potential difficulties that arise when detecting the flux from

an YBCO SQUID using an aluminium SQUID. Experiments on the system described will give an indication of how the superconducting properties of micron sized YBCO grain boundary Josephson junctions are affected by the capping and insulating layers proposed. Experiments will give information on the electrical insulation properties of the insulating material and its transparency for magnetic fields. It will also tell whether it is possible to fabricate aluminium junctions using shadow evaporation on the rough surface of a thermal evaporated insulator to make read-out SQUID.

If the technology turns out to work, similar experiments may be repeated using submicron HTS grain boundary Josephson junction. Successful experiments may open the door for a novel technique for fabricating HTS flux qubits and readout devices on the same chip.

## 2.1 Aim and Objective

The project was originally divided into four steps, where each step is taking the project closer to the main objective. Here the second and third steps have been merged together. In order to more easily fulfill the objectives each objective has one or more targets. The targets should be measurable, have a time limit and take the need of resources into consideration.

The main objective of the thesis is to:

Design, fabricate and investigate a device consisting of an YBCO SQUID grown on a STO substrate surrounded by an Aluminum SQUID on the same substrate, intended to be used to detect and measure the induced flux from a known current in the YBCO SQUID at 300 mK using the surrounding aluminum SQUID.

### 2.1.1 Step I. Fabrication and characterization of aluminium SQUIDs

The first steps relies on the knowledge and the results from the course modelling and fabrication of micro/nano devices, FKA 190, spring 2003. A design and preliminary process parameters were already proposed and documented.

The objective of the first step is thus the same as in the and is given below:

Propose and document a method for fabricating aluminum DC-SQUIDS. Fabricate and measure the characteristics of the aluminum DC-SQUIDS. The aluminium dc-SQUIDS should fulfill the demands for flux-qubit read-out.

In order to fulfill the objective the following targets are stated:

- Determine critical current, retrapping current, resistance and capacitance of the aluminum SQUIDS.
- Find suitable parameters for the shadow evaporation
- Find suitable parameters for the electron beam lithography.
- If needed, propose a set of modified process parameters

### **2.1.2 Step II. Study of insulating and capping materials**

The device described in the main objective is a multilayer device. YBCO is grown on an insulating STO substrate. The aluminium structures should be deposited on top of the YBCO structures. Between the YBCO and the aluminium an insulating layer has to be deposited in order to avoid short-circuit. The insulating layer should also act as a protection/capping layer, protecting the YBCO from degradation over time and during the other fabrication steps.

The objective of the second step is given below:

Find a two material combination that would act as an insulating layer between the YBCO and the Aluminum, that prevent short-circuit, is smooth, protects the YBCO film/pattern from degradation and that does not degrade the properties of the YBCO film/pattern.

In order to fulfill the objective the following targets are stated.

- Chose appropriate insulators and capping material.
- Determine how the critical temperature of the YBCO is affected when a layer of the insulator is deposited on top of the YBCO and if it changes during the aluminium patterning process.

- Determine the surface roughness of the insulator.
- Determine how thick the insulating layer has to be in order to prevent short-circuit between the YBCO and the Aluminum.
- Be able to perform the patterning process of YBCO

### **2.1.3 Step III. Read-out of an YBCO SQUID using a surrounding aluminium SQUID**

The final step of the project is to put a grain boundary SQUID made of YBCO on a STO bi-crystal substrate and then deposit capping and insulating layer on top of the YBCO structures. Finally an under-damped aluminum SQUID that surrounds the HTS SQUID is fabricated on top of the structure. The induced field from a known signal in the YBCO SQUID should be detected by the Aluminum SQUID.

The objective of the third step is:

Model and fabricate a circuit consisting of a YBCO grain boundary SQUID and an under-damped surrounding aluminum SQUID and detect a known signal, excitation, in the YBCO SQUID using the Al-SQUID via the inductive coupling.

In order to fulfill the objective the following targets are stated.

- Design a YBCO grain-boundary SQUID suitable for 300 mK.
- Fabricate a YBCO grain-boundary SQUID suitable for 300 mK.
- Find the characteristics of the SQUID
- Fabricate aluminum dc-SQUIDs surrounding the YBCO SQUID on the capping and insulating layer.
- Measure the induced flux from the signal in the YBCO SQUID with the aluminium SQUID.

# Chapter 3

## Theoretical introduction

A system of weakly interacting particles can be described by the ordinary Schrödinger equation.

$$i\hbar \frac{\partial \psi}{\partial t} = H\psi \quad (3.1)$$

where  $\psi = |\psi(\mathbf{r}, t)|e^{i\chi(\mathbf{r}, t)}$  is the complex wavefunction of a particle. In the stationary case  $|\psi|$  is assumed to be constant and the Hamiltonian,  $H$ , in equation 3.1 can be replaced by its eigenvalue,  $\epsilon$ . Equation 3.1 now takes the simpler form:

$$\hbar \frac{\partial \chi(\mathbf{r}, t)}{\partial t} = -\epsilon \quad (3.2)$$

A consequence of equation 3.2 is that it is possible to describe the dynamics of the particle only by considering its phase.

In a superconductor two electrons with opposite momenta form a bound state, a Cooper pair. Thus the net spin of the Cooper pair is zero and the Cooper pairs obey Bose-Einstein statistics. At low temperatures the Cooper pairs are condensed into the lowest energy level and as a result they all have identical time derivatives of their phase. Moreover the Cooper pairs are fairly large,  $\xi_0=1600$  nm in aluminium and  $\xi_0=2.5$  nm in YBCO, [16], which is much larger than the spacing between the pairs. The overlap and the identical energy of the Cooper pairs imply that all pairs at a given point in a superconductor turn out to be "phase-locked" and can be described by a single wavefunction  $\psi$ . This wavefunction is called the order parameter.

### 3.1 DC Josephson effect

Consider two superconductors connected by a thin insulating layer, [17]. Define  $\psi_L$  and  $\psi_R$  as the wavefunction/order parameters of the left and the right superconductor. The dynamics of the junction is given by the following coupled Schrödinger equations.

$$\begin{aligned} i\hbar \frac{\partial \psi_L}{\partial t} &= \epsilon_L \psi_L + K \psi_R \\ i\hbar \frac{\partial \psi_R}{\partial t} &= K \psi_L + \epsilon_R \psi_R \end{aligned} \quad (3.3)$$

Here,  $\epsilon_L$ ,  $\epsilon_R$  is the lowest energy eigenvalue of the left and the right superconductor and  $K$  represents the coupling across the barrier. Denoting the density of Cooper pairs and the phase in the superconductors by  $n_L$ ,  $\chi_L$  respectively  $n_R$ ,  $\chi_R$  and inserting the ansatz  $\psi_L = \sqrt{n_L(\mathbf{r}, t)} e^{i\chi_L(\mathbf{r}, t)}$ ,  $\psi_R = \sqrt{n_R(\mathbf{r}, t)} e^{i\chi_R(\mathbf{r}, t)}$  into equation 3.3 one gets.

$$\begin{aligned} \hbar \frac{\partial n_L}{\partial t} &= -\hbar \frac{\partial n_R}{\partial t} = 2K \sqrt{n_L n_R} \sin(\chi_R - \chi_L) \\ -\hbar \frac{\partial}{\partial t} (\chi_R - \chi_L) &= \epsilon_2 - \epsilon_1 \end{aligned} \quad (3.4)$$

The time derivative of the density of Cooper-pairs is nothing else then the charge transport. If a voltage is applied across the junction the energy level will shift  $\epsilon_2 - \epsilon_1 = 2eV$  due to the charge of a Cooper pair. Defining the maximum current, the critical current  $I_c$  as  $I_c = 2K \sqrt{n_L n_R} / \hbar$  and the phase difference or the Josephson phase  $\phi$  as  $\phi = \chi_R - \chi_L$  the equations governing the Josephson effect is obtained.

$$\begin{aligned} I &= I_c \sin(|\phi|) \\ \frac{\partial \phi}{\partial t} &= \frac{2e}{\hbar} V = \frac{2\pi}{\Phi_0} V \end{aligned} \quad (3.5)$$

In the stationary case,  $\partial \phi / \partial t = 0$ , equation 3.5 has two solutions:

$$\begin{aligned} \phi &= \phi_n = \arcsin(I/I_c) + 2\pi n \\ \phi &= \phi'_n = \pi - \arcsin(I/I_c) + 2\pi n \end{aligned} \quad (3.6)$$

each of them corresponds to zero voltage i.e. the S-state. Equation 3.6 shows that the current in the S-state consists of an infinite number of harmonics. Thus, in the general case 3.5 should be expressed as follows:

$$I = I_c \sin(\phi) + \sum_{m=2}^{\infty} I_m \sin(m\phi) \quad (3.7)$$

In most cases all terms except the first one can be neglected [18], whereas in certain high- $T_c$  junctions with high mismatch angle all terms except the first two ones can be neglected, [19]. The presence of a second harmonic is due to the d-wave symmetry of the material. The magnitude of the first harmonic in such a material can be approximated by trigonometry, [19].

$$I_{c,1} = I_a \cos 2\theta_1 \cos 2\theta_2 + I_b \sin 2\theta_1 \sin 2\theta_2 \quad (3.8)$$

Where  $\theta_1$  ( $\theta_2$ ) denotes the angle between the normal to the grain boundary and the  $a$ -axis in the electrode and the coefficients  $I_a$  and  $I_b$  are considered to be functions of the barrier strength, temperature etc. It is seen from equation 3.8 that  $I_{c,1} \neq 0$  for  $|\theta_1 - \theta_2| \neq 45^\circ$ .

## 3.2 AC Josephson effect

According to equation 3.5 current can not be carried through a junction by the supercurrent alone if it exceeds the critical current  $I_c$ . A more complete description is required. In the RCSJ (resistively and capacitively shunted junction) model the junction is modelled by a circuit where an ideal Josephson junction is shunted by a resistor and a capacitor. The resistance causes dissipation in the finite voltage regime without affecting the lossless dc regime, while the capacitor reflects the geometric shunting capacitance between the two electrodes.

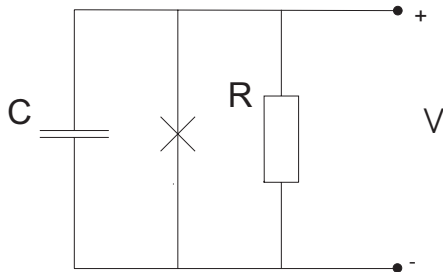


Figure 3.1: Equivalent circuit of a Josephson junction using the RCSJ model, (Resistively and Capacitively Shunted Junction)

The time dependence of the phase  $\phi$  in the presence of an externally supplied bias current can be derived by equating the bias current to the total junction current from the three parallel channels.

$$I = I_c \sin \phi + \frac{V}{R} + C \frac{\partial \phi}{\partial t} \Leftrightarrow \beta_c \frac{\partial^2 \phi}{\partial \tau^2} + \frac{\partial \phi}{\partial \tau} + \sin \phi = \frac{I}{I_c} \quad (3.9)$$

where  $V$  is eliminated in favor of  $\phi$  and:

$$\beta_c = \frac{2e}{\hbar} I_c R^2 C = \frac{2\pi}{\Phi_0} I_c R^2 C \quad (3.10)$$

$$\tau = 2\pi f_c t = \frac{2\pi}{\Phi_0} I_c R \quad (3.11)$$

here  $f_c$  is the Josephson frequency. The damping parameter,  $\beta_c$  was introduced by Stewart and McCumber, [20] and [21] and is referred to as the Stewart-McCumber parameter. An approximate expression for the Stewart-McCumber parameter for a Josephson junction is given in equation 3.12, [22], [23]. The formula is valid for  $\beta_c \simeq 1$  and  $I_r$  denotes the retrapping current.

$$\beta_c = \frac{2 - (\pi - 2)(I_r/I_c)}{(I_r/I_c)^2} \quad (3.12)$$

Qualitative insight into the junction dynamics described by the RCSJ model can be obtained from the so called "tilted washboard" model which describes a mechanical analogue, [24]. A particle of mass  $(\hbar/2e)^2 C$  moves along the  $\phi$  axis in an effective potential

$$U(\phi) = -E_J \left( \frac{I}{I_c} + \cos(\phi) \right) \quad (3.13)$$

subjected to a viscous drag force  $(\hbar/2e)^2 (1/R) \partial \phi / \partial t$ . Here,  $E_J = (\hbar/2e) I_c$ , denotes the Josephson energy. Notice that for  $I > I_c$  no stable equilibrium exist, the particle is in the R state. When  $I < I_c$  the particle is moving back and forth in a minimum, it is in the S-state. When the particle has a large inertia compared with the damping of the system, large mass, it will continue to move down along the contour if it gets excited until the current is less than the retrapping current, we get hysteresis.

More sophisticated methods such as the nonlinear resistive (RSJN) model, where the resistance is piecewise linear and depends on the voltage, and the TJM (Tunnel Junction Microscopic) model exist. However, for this qualitative purpose the RSCJ model is sufficient.

In the high damping limit where  $\beta \ll 1$ , the effective inertia of the quasi-particle is small. As a consequence only the S-state is possible for  $|I| < I_c$

and at  $|I| > I_c$  only the R-state is possible. The I-V curve is nonhysteretic, i.e. the current is single-valued. The I-V of the junction is approximately described by the following equations.

$$V = 0 \quad ; \quad I < I_c \quad (3.14)$$

$$V = R_n I_c \sqrt{\frac{I^2}{I_c^2} - 1} \quad ; \quad I > I_c \quad (3.15)$$

The I-V characteristic for an over damped junction,  $\beta_c=0.001$ , is exemplified in figure 3.2. It could be obtained by solving equation 3.9 for a set of bias currents or by using the relation above.

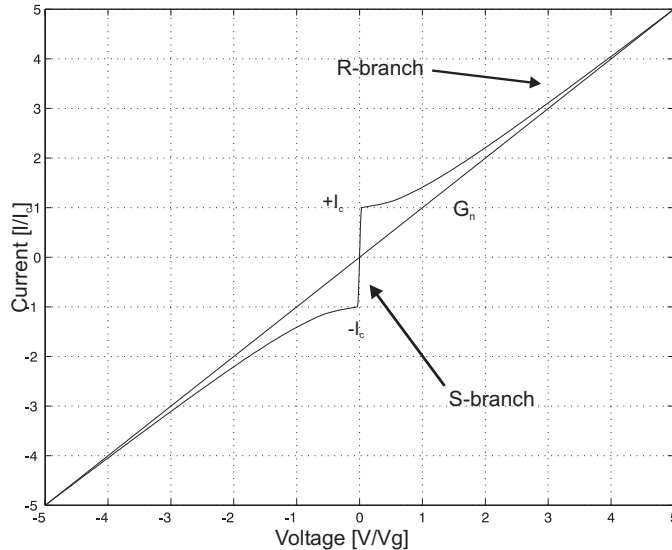


Figure 3.2: I-V characteristics of an over damped SQUID,  $\beta = 0.001$ . The figure is obtained by the RCSJ model. Here  $G_n$  denote the normal conductance which is the inverse of the normal resistance,  $R_n = G_n^{-1}$

In the low damping limit where  $C$  is large and  $\beta \gg 1$ , the I-V curve becomes hysteretic. At  $|I| = I_c$  the quasiparticle switches from the S branch of the I-V curve to the R branch. The process can be approximately modelled by the RCSJ model, equation 3.9 if the supercurrent component, the sine-term, is neglected. The junction is then modelled by a capacitor and resistor in parallel, and obeys similar dynamics as a capacitor. When the

current is reduced below  $I_c$  at  $V = V_g$  the quasiparticle switches back to the S branch from the R branch when the retrapping current  $I_r$  is obtained.

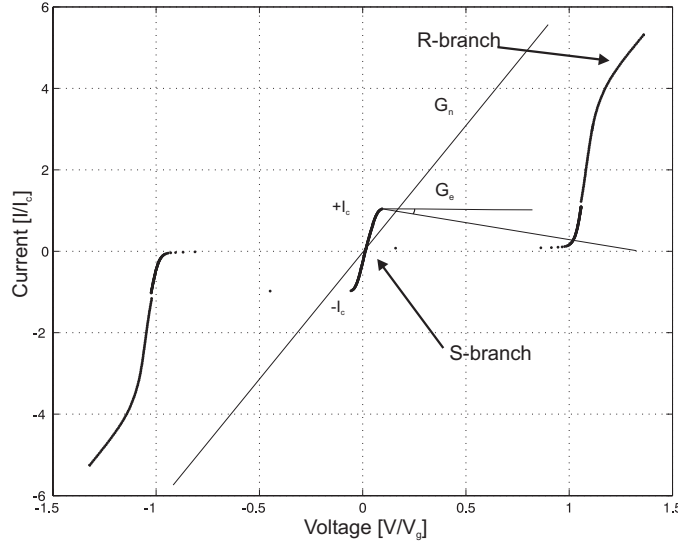


Figure 3.3: I-V characteristics of an under damped SQUID,  $\beta \gg 1$ . The current and the voltage are normalized,  $I/I_c$  and  $V/V_g$ . The normal conductance,  $G_n$  is inverse of the normal resistance.  $G_e$  is the leakage conductance. The leakage conductance is a measure of the damping of the junction. (The slope of the supercurrent is due to a resistance in series during the measurements.)

Figure 3.3 illustrates how the current switches from the S branch to the R branch at  $I = |I_c|$  and how it switches back to the S branch at  $I = I_r \simeq 0$ .

### 3.3 Superconducting QUantum Interference Device, SQUID

Consider a device consisting of two Josephson junctions coupled in parallel. Such a device is called a Superconducting QUantum Interference Device, SQUID. SQUIDS are based on the principle of quantum interference. The critical current is modulated by the flux enclosed by the loop in units of flux quanta,  $\Phi_0$ . Thus SQUIDS can be viewed as extremely sensitive flux-to-voltage converters. A sketch of a SQUID is presented in figure 3.4.

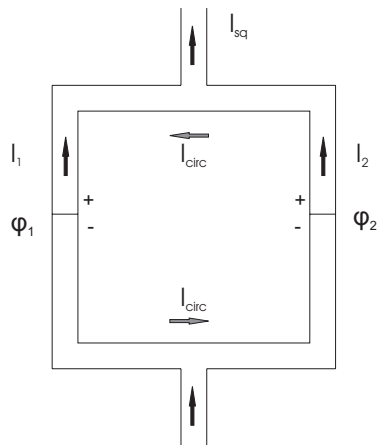


Figure 3.4: Two Josephson junctions in parallel form a SQUID. The current and the phase in the left branch is denoted by index 1 and 2 in the right branch.

The current in the left and right superconductor in figure 3.4 is according to equation 3.7 given by:

$$I_1 = I_{c,1} \sin(\phi_1) + I'_{c,1} \sin(2\phi_1) = I_{c,1} [\sin(\phi_1) + \alpha_1 \sin(2\phi_1)] \quad (3.16)$$

$$I_2 = I_{c,2} \sin(\phi_2) + I'_{c,2} \sin(2\phi_2) = I_{c,2} [\sin(\phi_2) + \alpha_2 \sin(2\phi_2)] \quad (3.17)$$

here the first two harmonics are taken into consideration,  $\alpha_i = I'_{c,i}/I_{c,i}$ . The inclusion of the second harmonic is needed when working with some HTS junctions with high mismatch angle. The equations governing the SQUID dynamics are derived by introducing the compound variables;  $I_{sq}$ ,  $I_{circ}$ ,  $\phi$ , and  $\theta$ .

$$\phi = \frac{\phi_1 + \phi_2}{2} \leftrightarrow \phi_1 = \phi - \frac{\theta}{2} \quad (3.18)$$

$$\theta = \phi_2 - \phi_1 \leftrightarrow \phi_2 = \phi + \frac{\theta}{2} \quad (3.19)$$

$$I_{sq} = I_1 + I_2 \leftrightarrow I_1 = \frac{1}{2}I_{sq} - I_{circ} \quad (3.20)$$

$$I_{circ} = \frac{I_2 - I_1}{2} \leftrightarrow I_2 = \frac{1}{2}I_{sq} + I_{circ} \quad (3.21)$$

Here,  $\phi$  represents the average phase of the SQUID and  $I_{sq}$  the total current through the SQUID. These two variables describe the behavior of a SQUID as if it were a single junction.

The parameters  $\theta$  and  $I_{circ}$  shows where the SQUID differs from a junction. The phase difference  $\theta$  is dependent on the total flux  $\Phi$  threading the loop. By summing up phase contributions from the flux and the junctions taking advantage of the  $2\pi$  periodicity of the order parameter one gets:

$$\oint \nabla\phi \cdot d\mathbf{l} = 2\pi n = \frac{2\pi}{\Phi_0} \oint \mathbf{A} \cdot d\mathbf{l} + \frac{m}{2e^3 n} \oint \mathbf{I} \cdot d\mathbf{l} - \theta \quad (3.22)$$

By choosing an integration path well inside the two superconductors the integral in the first term on the right hand side is recognized as the total magnetic flux  $\Phi$ . Since the current inside the superconductor is zero, there will be no contribution from the second term and the expression can be simplified to:

$$2\pi n = \frac{2\pi}{\Phi_0} \Phi - \theta \Leftrightarrow \theta = \frac{2\pi}{\Phi_0} \Phi + 2\pi n' \quad (3.23)$$

Equation 3.23 is telling us that the current through the SQUID,  $I_{sq}$ , and the circulating current,  $I_{circ}$ , are modulated with a period of  $\Phi_0$ . Where  $\Phi_0 = h/2e$  is the quantum flux. The general expressions for  $I_{sq}$  and  $I_{circ}$  are obtained using equation 3.16 - 3.20.

$$\begin{aligned} I_{sq} = I_1 + I_2 &= (I_{c,1} + I_{c,2}) \sin(\phi) \cos(\theta/2) + (I'_{c,1} + I'_{c,2}) \sin(2\phi) \cos(\theta) \\ &- [(I_{c,1} - I_{c,2}) \cos(\phi) \sin(\theta/2) + (I'_{c,1} - I'_{c,2}) \cos(2\phi) \sin(\theta)] \end{aligned} \quad (3.24)$$

$$\begin{aligned}
I_{circ} &= \frac{I_2 - I_1}{2} = \frac{1}{2} [(I_{c,2} - I_{c,2}) \sin(\phi) \cos(\theta/2) + (I'_{c,2} - I'_{c,1}) \sin(2\phi) \cos(\theta)] \\
&\quad + \frac{1}{2} [(I_{c,2} + I_{c,1}) \cos(\phi) \sin(\theta/2) + (I'_{c,2} + I'_{c,1}) \cos(2\phi) \sin(\theta)] \quad (3.25)
\end{aligned}$$

If the critical currents of the two junctions are equal equation 3.24 and 3.25 simplifies to:

$$I_{sq} = I_1 + I_2 = 2I_c [\sin(\phi) \cos(\theta/2) + \alpha \sin(2\phi) \cos(\theta)] \quad (3.26)$$

$$I_{circ} = \frac{I_2 - I_1}{2} = I_c [\cos(\phi) \sin(\theta/2) + \alpha \cos(2\phi) \sin(\theta)] \quad (3.27)$$

For junctions where only the first harmonic contributes,  $\alpha = 0$  the second term in equation 3.26 and 3.27 cancels out. Notice that when the second harmonic is missing the absolute value of  $I_{sq}$  is maximized when  $\phi = \pi/2 + \pi n$  and  $\theta = 2\pi n$  while the absolute value of  $I_{circ}$  is maximized when  $\phi = \pi n$  and  $\theta = \pi n$ . When the second harmonic is present the extrema have to be determined using numerical techniques.

## 3.4 Electrical Insulation and Capping of YBCO

The oxygen content of  $YBa_2Cu_3O_{7-\delta}$  is extremely important for its superconducting properties. A small change of  $\delta$  may cause a drastic change of the critical temperature, [16]. Thus an insulating layer in a multi layer structure made up of YBCO should not just be insulating, it should not affect the superconducting properties of the YBCO, critical current etc, it is even preferable if it counteract oxygen diffusion.

### 3.4.1 Capping of YBCO

Silicon dioxide,  $SiO_2$  is a common insulator in semiconductor fabrication. In [27] the effects of a thick layer of silicon dioxide on top of YBCO FIB-junctions is studied. The study showed that the critical current of a 3  $\mu\text{m}$  wide and 300 nm thick YBCO FIB-junction on a MgO substrate decreased to about 60 % of its nominal value after a 600 nm thick layer of  $SiO_2$  was deposited on top of it using a sputtering method with Ar/ $O_2$  plasma. The study also showed that the critical temperature increased a little bit after

the deposition. This phenomena was also observed in [28].

STO is "friendly" to YBCO and has been used as insulating layer in YBCO multi layers, e.g. SuFETs, [25], [26]. Since SiO<sub>2</sub> may enhance oxygen diffusion it would be preferable to have a capping layer of another material closest to the YBCO. It has been shown in [26] and [29] that a capping layer of STO on top of the YBCO film prevents oxygen diffusion. However, according to [30] the STO should be deposited at low temperature in order to minimize oxygen diffusion during the process. Deposition at low temperatures also make it possible to use patterning techniques such as photo- and E-beam lithography.

### 3.4.2 Electrically insulating layer

If the intermediate insulating layer is considered to be thick, it can be approximately modelled by two Schottky diodes in series. According to [31] the following formula would give its characteristics.

$$J(V) = J_{st,1} \left[ \exp\left(\frac{eV}{kT}\right) - 1 \right] - J_{st,2} \left[ \exp\left(\frac{eV}{kT}\right) - 1 \right] \quad (3.28)$$

where  $J_{st,1}, J_{st,2}$  is the reverse-saturation current density of the two interfaces. Making the substitution,  $V' = V - V_{max}$  the R-V characteristics are described by;

$$R(V) = R_{max} \cosh^{-1} \left( \frac{eV'}{kT} \right), \quad (3.29)$$

where  $R_{max} = kT / (2Ae \sqrt{J_{st,1} J_{st,2}})$ .

# Chapter 4

## Design and experiment

According to section 2.1, the objective of this thesis is to: design, fabricate and investigate a device consisting of an YBCO SQUID grown on a STO substrate surrounded by an aluminum SQUID on the same substrate. The aluminium SQUID is intended to be used to detect and measure the induced flux from a known current in the YBCO SQUID at 300 mK.

This chapter has the intention to describe how the demands in the objective are met. In other words, how the experiment is performed, how the final setup and the devices of the final setup are designed in order to meet these demands.

A sketch of the experimental setup is presented in figure 4.1. A high- $T_c$  grain boundary YBCO SQUID is fabricated on a STO bicrystal. On top of the YBCO SQUID a single/multi layer of insulating/capping materials is deposited. A low- $T_c$  aluminium SQUID is fabricated on top of the insulator using shadow evaporation. The bottom YBCO SQUID can be current and flux biased so to maximize the circulating current of the SQUID. The circulating current will induce a flux. The induced flux can be detected by the upper aluminium SQUID by measuring its critical current  $I_{c,Al}$ .

The experiment will tell us how large is the inductive coupling between the SQUIDs and how well it corresponds to theoretical models. It will tell us if it is possible to put an insulator on top of an YBCO grain boundary SQUID without affecting the superconducting properties of the YBCO. It will tell us if it is possible to fabricate aluminium junctions on the rough surface, (by comparison with a Silicon wafer), of a thermally evaporated insulator. Finally the experiment will tell us if the proposed method is worth refining for future use.

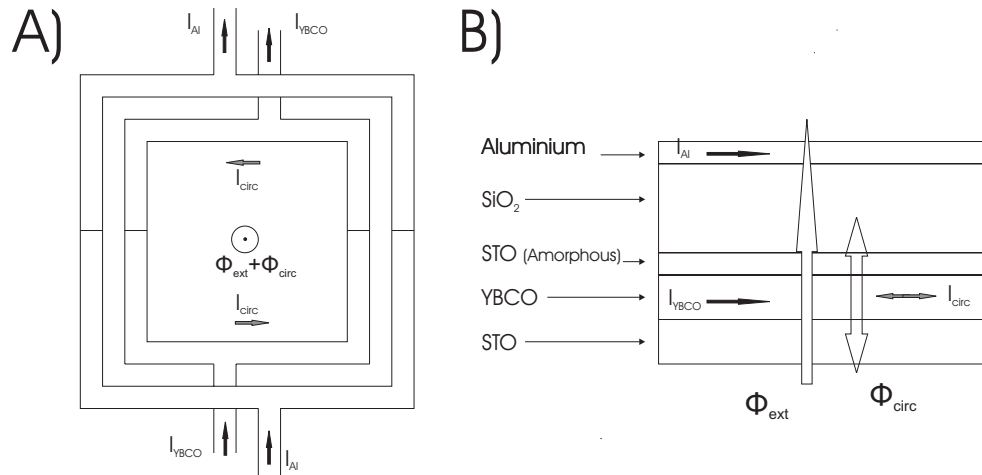


Figure 4.1: Sketch of the experiment setup. A) Top view of the setup. A YBCO grain boundary SQUID is surrounded by a aluminium SQUID separated by an intermediate insulating/capping layer. B) Side view of the setup showing the STO/YBCO/amorphous STO/SiO<sub>2</sub>/Aluminium multi layer.

## 4.1 Operation/Method

The proposed idea is realized in the experiment described below.

1. Determine the modulation of the critical current in an external magnetic field for both the SQUIDS.
  - Measure  $I_c(\Phi)$  for the aluminium SQUID.
  - Measure  $I_c(\Phi)$  for the YBCO SQUID.
  - Determine the period of modulation for the YBCO SQUIDS and the aluminium SQUIDS.
2. Determine the modulation of  $I_c(\Phi)$  for the aluminium SQUID
  - by driving a current through a YBCO coil.
  - by biasing the YBCO SQUID with a current and an external magnetic field generating a circulating current and inducing a flux.

## 4.2 Specification

In order to get the experiment working the devices in the setup has to fulfil certain requirements. This section specifies the requirements needed. The requirements are based on numerical and analytic calculations, recommendations given in relevant papers and rules of thumb given by researcher at QDP.

The **aluminium SQUIDs** should have the following properties:

- A high critical current,  $I_c > 100$  nA.
- A small self inductance,  $L_{Al} < 100$  pH.
- A small damping, Stewart McCumber parameter  $\beta_c \gg 1$ .

The critical current specified corresponds to a Josephson energy of 2.38 K, which is 8 times larger than the temperature where the measurements are performed. The current is measured with an accuracy of  $\Delta I_c \geq \pm 5$  nA, corresponding to a flux accuracy  $\Delta \Phi \simeq (\Delta I_c / I_c) \Phi_0$ . A low self inductance prevents magnetic hysteresis and flux fluctuations and an under damped SQUID has a faster response to flux changes.

The **YBCO SQUIDs** should have the following properties:

- A critical current,  $I_c > 50$   $\mu$ A.
- Self inductance,  $L_{YBCO}$ , less than 100 pH.

The YBCO SQUIDs should have a high critical current so that they are able to induce a large flux in the surrounding aluminium SQUIDs. The specified current corresponds to a needed mutual inductance of at least 8-16 pH between the two SQUIDs in order to be able to detect the direction of the circulating current. A low-angle bi-crystal should be used to get a high critical current and a simple current phase relation.

The **insulating material** should have the following properties:

- A resistance of minimum 1 M $\Omega$  in the relevant voltage regime of the proposed experiment and it should be transparent to low frequency EM-radiation.
- Have a smooth surface which enable high quality aluminium SQUID to be fabricated on top of it.
- Good sticking to STO, YBCO and aluminium

- It should not drastically degrade the superconducting properties of the YBCO.

The demanded resistance corresponds a leakage current of 1 nA per 1 mV. Thus, for moderate voltage differences the leakage currents would be smaller than the measurement accuracy. It is important that the intermediate layer does not degrade the superconducting properties of the YBCO. The critical current of a junction has to be high enough. The surface of the insulator also has to be smooth and metals deposited on top of it should have good adhesion. In order to link flux from the lower SQUID to the upper one the intermediate insulator has to have a permittivity close to unity.

The **final setup** should have an inductive coupling of, at least, 20 pH between the two SQUIDs that are separated by an insulator. A mutual inductance of 20 pH and a circulating current of 25  $\mu$ A will induce a flux corresponding to  $0.5\Phi_0$ .

### 4.3 Aluminium SQUIDs

Fabrication of the SQUIDs is the last step of a process consisting of approximately 50 process steps. For a good result it is important that the process has high yield and high reproducibility.

To develop the technology, the SQUIDs are first fabricated on silicon wafers. Process parameters and SQUID characteristics are determined. As a second step SQUIDs are fabricated on top of the intermediate layer. The process is modified to fit the new conditions which is the same condition as in the final configuration. The SQUIDs were characterized in measurements at 300 mK for both these cases. For measurement setup see chapter 6. The critical current,  $I_c$ , the superconducting gap,  $\Delta$ , the normal resistance,  $R_n$ , the retrapping current,  $I_r$  and the Stewart-McCumber parameter,  $\beta_c$  are determined.

The Ambegaokar-Baratoff formula, equation 4.1, gives the temperature dependence of  $I_c$  in a SIS junction.

$$I_c R_n = \frac{\pi \Delta}{2e} \tanh \frac{\Delta}{2k_b T} \quad (4.1)$$

The band gap for an aluminium film with  $T_c=1.6$  K at 0 K is 0.237 meV,  $\simeq 0.25$  meV, in the weak coupling limit, [16]. Thus for an ideal junction

with  $I_c=100$  nA the resistance should be  $3.5$  k $\Omega$ . The capacitance for an aluminium SIS junction is approximately  $45$  pF/ $\mu\text{m}^2$ , [32].

### 4.3.1 Aluminium SQUID design

According to the specification in section 4.2 the SQUIDs should have a critical current larger than  $100$  nA, a self inductance less than  $100$  pH and a Stewart McCumber parameter larger than unity. Two different loop designs are proposed, a large,  $36$   $\mu\text{m}$  x  $28$   $\mu\text{m}$ , and a small,  $20$   $\mu\text{m}$  x  $20$   $\mu\text{m}$ . The depth of the junctions, the overlap, is kept fixed,  $250$  nm, but their width is varied,  $0.5$   $\mu\text{m}$ ,  $0.7$   $\mu\text{m}$ ,  $1$   $\mu\text{m}$  and  $1.5$   $\mu\text{m}$ . The junction size that will show the best reproducibility together with a high critical current will be chosen for the final setup. The circuit design is presented in figure 4.2.

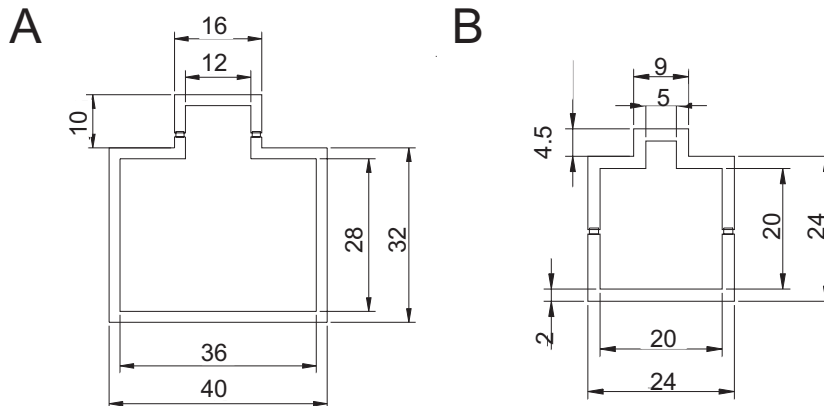


Figure 4.2: SQUID design. Left. Large  $36$   $\mu\text{m}$  x  $28$   $\mu\text{m}$  SQUID. Right: Small  $20$   $\mu\text{m}$  x  $20$   $\mu\text{m}$  SQUID. The junction depth, overlap, is kept fixed,  $250$  nm, but the junction width is varied,  $0.5$   $\mu\text{m}$ ,  $0.7$   $\mu\text{m}$ ,  $1$   $\mu\text{m}$  and  $1.5$   $\mu\text{m}$

According to equation 4.1 a critical current of  $100$  nA corresponds to a normal resistance of  $3.5$  k $\Omega$ . Keeping in mind that the relation is only valid for ideal junctions the resistance is likely to be lower.

The self inductance is calculated numerically by the software 3DMLSI. The self inductance for the two proposed designs in figure 4.2 is  $97.9$  pH for the large one and  $53.1$  pH for the smaller one.

The proposed design will most likely meet the specification. Both designs have a self inductance below  $100$  pH, which according to [24] will prevent

magnetic hysteresis and noise. Depending on how good is the approximation for the conductance, all proposed junctions will have Stewart-McCumber parameter larger than unity,  $\beta_c > 1$ , i.e. under-damped.

### Shadow evaporation

The aluminium junctions are fabricated by shadow evaporation. Metal is evaporated at angle  $-\theta$ , then the surface is oxidized in an oxygen atmosphere and finally metal is evaporated at an angle  $+\theta$ . In figure 4.3 the junction is sketched.

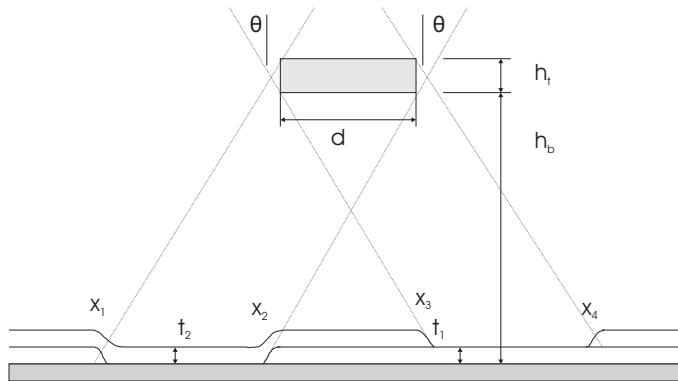


Figure 4.3: Shadow evaporation. Here,  $h_b$  represents the thickness of the bottom resist layer,  $h_t$  the thickness of the top resist layer,  $d$  the width of the resist bridge and  $\theta$  the evaporation angle.

The length of the junction is given by the equation:

$$l_{junc} = x_3 - x_2 = \frac{t_1}{\cos \theta} + 2(h_b - t_1) \tan \theta - d \quad (4.2)$$

where  $d$  is the length of the bridge,  $t_1$  the thickness of the bottom layer,  $h_b$  the thickness of the bottom e-beam resist layer, and  $\theta$  the evaporation angle.

When the aluminium is exposed to oxygen an insulating aluminium oxide,  $Al_2O_3$  forms on the surface. The thickness of the oxide layer is proportional to  $p^\alpha \log t$ , using an ideal gas approximation. The junctions are short circuited if they are not oxidized long enough. At least one monolayer has to be formed on the surface to prevent short circuit. A short circuit also occurs when particles diffuse away and make a contact over the junction. The spacings  $x_2 - x_1 = x_4 - x_3$ , see figure 4.3, equals  $d$  for moderate angles but if there is a rough angle resolution of the source particles may diffuse and cause a short circuit as described above.

## 4.4 YBCO SQUIDS

The flux qubit design proposed in [12] uses  $0^\circ/45^\circ$  GBJJ. In this study  $0^\circ/30^\circ$  GBJJ are used. The later ones have a simpler CPR and a higher critical current, [19]. Both properties simplify this experiment. Two different designs of YBCO grain boundary SQUIDS are proposed.

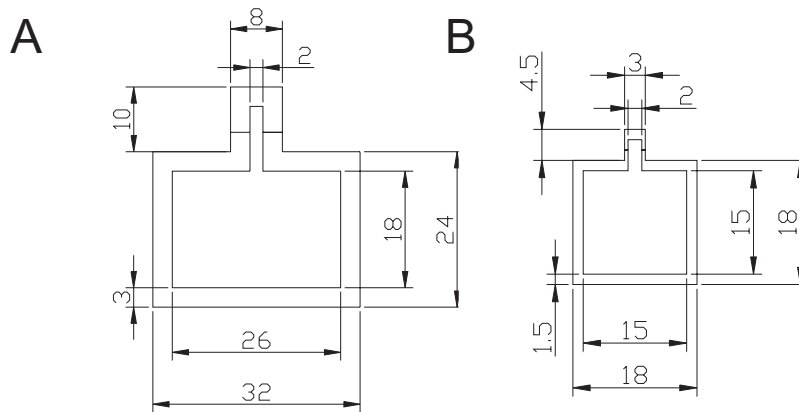


Figure 4.4: SQUID design. Left:  $26 \mu\text{m} \times 18 \mu\text{m}$  SQUID with a junction width of  $3 \mu\text{m}$ . Right:  $15 \mu\text{m} \times 15 \mu\text{m}$  SQUID with a junction width of  $0.5 \mu\text{m}$ . The grain boundary is located at the top of the loop in order to build a device similar to the one proposed in [12].

The large SQUID has a junction width of  $3 \mu\text{m}$  and an area of  $26 \mu\text{m} \times 18 \mu\text{m}$ . The smaller one has an area of  $15 \mu\text{m} \times 15 \mu\text{m}$  and its junctions are  $0.5 \mu\text{m}$  wide. The self inductances of the SQUIDS are  $55.8 \text{ pH}$  and  $39.4 \text{ pH}$ . The junctions are placed at the top of the loops in order to test the idea on a system more comparable with the one proposed by [12]. According to [33] the large junctions will have a critical current of the order of hundreds of micro amperes and the small ones of the order of tens of micro amperes. The characteristics of the SQUIDS will be determined before and after deposition of any insulating/capping layer.

## 4.5 Capping and Insulating layer

The intermediate layer between the YBCO structures and the aluminium structures should consist of two materials. A bottom layer of amorphous STO deposited at room temperature acting as capping layer that prevents oxygen diffusion from the YBCO, and a top layer of silicon dioxide deposited

using e-gun evaporation that act as a insulator. Because it is unlikely that one will get exactly the correct stoichiometry for the silicon dioxide during the evaporation we hereinafter refer to it as  $\text{SiO}_{2-x}$ .

### 4.5.1 Experiments

#### R-V characteristics

The insulating properties of the insulator silicon dioxide,  $\text{SiO}_{2-x}$  are studied at 4.2 K by measuring the IV curve for YBCO/ $\text{SiO}_2$ /Al junctions of various sizes. The device used to realize the experiment consists of YBCO lines of thickness 1, 2, 4, 6, 10, and 15  $\mu\text{m}$  as bottom layer. A 0.55  $\mu\text{m}$  thick intermediate layer of  $\text{SiO}_{2-x}$  and a top layer consisting of orthogonal aluminium lines of thickness 1, 2, 4, 6, 10, and 15  $\mu\text{m}$ . Where the lines intersect each other 24 junctions with 20 different areas in the range 1  $\mu\text{m}^2$  to 225  $\mu\text{m}^2$  are formed on the chip . The setup is presented in figure 4.5.

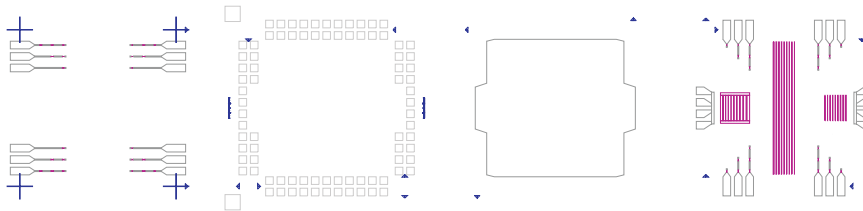


Figure 4.5: The image shows the four layers of the chip. From left to right; a) The YBCO pattern consisting of four group of horizontal strips, b) the gold pads, c) the insulating layer and d) the layer of vertical aluminium strips.

At 4.2 K the aluminium is not superconducting but the resistance is low and constant. Thus the experiment will give us an idea of the strength of the insulator.

#### Smoothness and adhesion

A couple of test chips are fabricated for studies of the smoothness and the adhesion of amorphous STO and  $\text{SiO}_2$ . Silicon and STO substrates will be used. Patterns for the insulator are made by photolithography in order to test if the technique is suitable for this purpose.

Atomic force microscope are used for studies of the surface morphology of the materials. The roughness of amorphous STO deposited on top of STO

and SiO<sub>2</sub> deposited on top of amorphous STO is compared with the roughness of a STO substrate and a Silicon wafer.

The adhesion are tested by placing the chip in a beaker of IPA in an Ultra Sonic bath. The ultra sound pulses will shake the chip and give a qualitative estimate of the adhesion strength. These sub-experiments enable a study of the possibilities of using photolithography and lift-off for depositing these materials.

## Degradation

The two component insulator/protection layer, amorphous STO/SiO<sub>2-x</sub> may degrade the superconducting properties such as the critical current,  $I_c$  and the critical temperature,  $T_c$  of the YBCO SQUIDS. In order to determine the magnitude of such degradation the properties of the HTS SQUIDS are measured before any insulator is deposited on top of them and when the chip got an amorphous STO/SiO<sub>2-x</sub> layer and aluminium SQUIDS. The experiment will tell whether the insulator is a good choice or not for YBCO. It will also enable studies of the capping qualities of the materials.

## 4.6 Final design

According to equation 3.27 the circulating current in the the YBCO SQUID is maximized when  $\theta/2 = \pi/2$  and should thus be biased with an external magnetic field equal to  $B_{ext} = A_{YBCO}\Phi_0/2$ . Only the first harmonic is taken into consideration for the YBCO SQUIDS with 0°/30° grain boundary junctions. If the area of the surrounding aluminium SQUID is chosen so that,  $A_{Al} = 3/2A_{YBCO}$ , the current through it will equal 1/2 of its maximum value at this external B-field.

Flux induced by the circulating current in the YBCO SQUID,  $\Phi_{circ} = LI_{circ}$ , will couple to the surrounding aluminium SQUID and modulate its critical current.

$$I_{sq,Al} \simeq 2I_{c,Al} \sin \phi_{Al} \cos \left( \frac{\pi}{3} + \pi \frac{\Phi_{circ}}{\Phi_0} \right) \quad (4.3)$$

According to equation 4.3  $I_{sq,Al}/2I_{c,Al} = 1/2$  for  $\Phi_{circ}/\Phi_0 = 0$ , 1 for  $-1/3$ ,  $1/\sqrt{2}$  for  $-1/12$ ,  $(\sqrt{6} - \sqrt{2})/4 \sim 0.25$  for  $-1/12$  and 0 for  $2/3$ .

In 4.3 and 4.4, designs for aluminium and YBCO SQUIDs are proposed. The final experimental configuration is presented in figure 4.6.

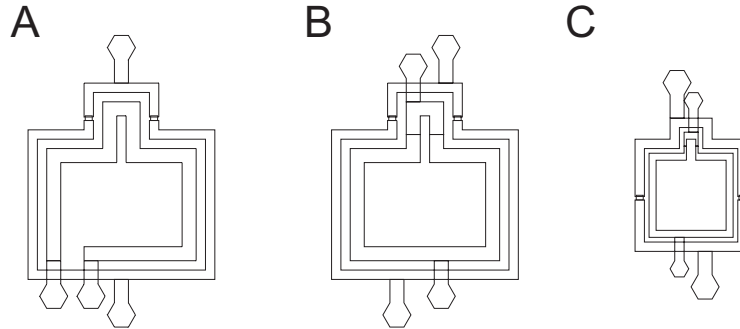


Figure 4.6: Final configuration. On each chip configuration B that consists of large SQUIDs are repeated six times, configuration C with small SQUIDs three times and configuration A with YBCO coil structure instead of a SQUID appears three times. The area of the surrounding aluminium SQUID is  $3/2$  times as big as the area of the inner YBCO device.

At each chip configuration B is repeated six times, configuration C three times and configuration A with YBCO coil structure instead of a SQUID appears three times. However, at two positions configuration A appears with a large surrounding aluminium SQUID and at one position with a small one. YBCO SQUIDs are replaced by coils in three out of 12 positions because of their higher reliability.

The two left most structures in figure 4.6 have a mutual inductance of 28 pH and the right most 19.8 pH. The mutual inductance is computed using the software 3DMLSI. The leads of each device are placed symmetric around the center of the device so that the left and right branch of the device have the same inductance.

# Chapter 5

## Sample Fabrication

All samples discussed in this thesis have been fabricated in the cleanroom facilities of the MC2 process lab at Department of Microtechnology and Nanoscience, Chalmers University of Technology, Göteborg.

### 5.1 Film Deposition and Characterization

YBCO films were grown by pulsed laser deposition on single and  $0^\circ/30^\circ$  bicrystal STO substrates. A pulsed laser beam is fired at a YBCO target situated in a vacuum chamber facing the substrate, which is attached to a heater with silver paste. When the target is hit by the laser beam, some material is ablated and is deposited on the substrate. The system used on-axis configuration. The following set of parameters was used for the final bicrystal film, substrate temperature  $780^\circ\text{C}$ , amount of pulses 5000, oxygen pressure during deposition, 0.5 mbar, and a substrate-to-target distance, 55 mm. The temperature was ramped down by  $20^\circ\text{C}$  per minute in an oxygen atmosphere of 900 mbar and then a 30 nm thick layer of gold was ablated under vacuum at room temperature, (16000 pulses).

The critical temperature  $T_c$  of the film was determined by a susceptibility measurement. A film is placed between two coils and the mutual inductance between the coils is measured as a function of temperature. When the film becomes superconducting, the mutual inductance between the coils is lowered due to screening currents induced in the film. The width and the shape of the transition gives additional information about the uniformity and quality of the film.

The crystallographic structure of the films was investigated by x-ray diffraction, XRD. From this measurement information about the film quality and about the occurrence of unwanted phases can be extracted. The surfaces of the films were investigated by optical microscope and atomic force microscope.

## 5.2 Pattern formation in YBCO films

This process was used for making YBCO SQUIDs and for YBCO pattern used in tests of various insulators. The YBCO films were patterned using a hard mask of carbon. Amorphous carbon has a very low ion beam etching rate compared to YBCO, approximately 1:5. Since amorphous carbon can not be patterned directly by an electron beam, the devices have to be patterned on a NiCr mask and transferred to the amorphous carbon layer. The YBCO film is then milled by a beam of argon ions. The procedure is described in more detail in [13] and [34].

The grain boundary of the bi-crystal is located by optical inspection using fine rulers, deposited at the same time as the alignment marks and the gold pads. A precision of approximately  $\pm 500$  nm is achieved. The device drawing is modified according to the observed grain boundary position. A 150 - 160 nm thick layer of amorphous carbon is deposited using electron gun evaporation. Since the quality of the carbon film depends on the oxygen content in the chamber, the film is deposited at low pressure,  $2 - 4 \cdot 10^{-7}$ . The pressure is decreased even more by evaporating titanium in the chamber with the shutter closed.

The patterning of devices onto the amorphous carbon mask was done by electron beam lithography. A two layer resist was used. As bottom layer a 300 nm thick layer of 10 % Copolymer PMAA in Ethyl Lactate and as top layer a 90 nm thick layer of ZEP520 diluted in anisole thinner 1:2. The resists are spun at 6000 rpm and 3000 rpm and baked at 135 °C for 5 min and 10 min respectively. A dose of  $110 \mu\text{C}/\text{cm}^2$  was used. The dose was adjusted according to the size of the features and proximity effect. Small structures were patterned by the fifth lens of a JEOL JBX-3DII EBL system at a current of 30 pA giving a spot size of 10 - 20 nm. Larger structures were patterned with the fourth lens at a current of 10 nA giving a spot size of 200 nm. The top layer is developed for 45 s. in Oxylene and the bottom layer for 8 min in ECA:Ethanol 1:5. The chip is rinsed in IPA and blown dry after each development.

A 50 nm thick film of NiCr is deposited using electron gun evaporation and lift-off is done in warm acetone. After lift-off an oxygen plasma is used to etch the amorphous carbon that is not protected by the NiCr mask. In such a way the pattern is transferred to the carbon mask. The unmasked YBCO is then etched by an argon ion beam, (400 eV, 0.1 mA/cm<sup>2</sup>). Low current density and cooling is used to minimize degradation. The etching time is approximately 2 h. 30 min. The residual carbon is removed in the same way as described above. Finally, the remaining Au capping layer is removed by ion milling at reduced kinetic energy, (200 eV and 0.1 mA/cm<sup>2</sup>).

## 5.3 Aluminium SQUIDs

Aluminum SQUIDs have been fabricated on Silicon wafers and on top of STO/YBCO/amorphous STO/SiO<sub>2</sub> multilayered chips. The procedure is slightly different in these cases. When SQUIDs are fabricated on a multi layer chip it is usually the last process step. A few adjustments have to be done in order to minimize degradation of the YBCO and to fit the geometry of the chip. When fabricating silicon wafers a matrix of chips is done at the same time. The matrix is diced into chips which are processed separately.

### 5.3.1 Gold pads and Alignment marks using photolithography

Photolithography was used to produce alignment marks, contact pads and some larger structures on silicon wafers and STO substrates. A layer of LOL2000 resist is spun on the wafer/chip at 3000 rpm for 200 - 250 nm thickness and is baked on a hotplate for 5 min at 130° C. On top of the LOL layer a layer of Shipley S-1813 photoresist is spun at 4000 rpm for approximately 1.3 μm thickness and is baked for 2 min at 110° C. The LOL - layer gives an undercut that prevents bad lift-off. The wafer/chip is exposed with UV-light through a soda lime glass photolithography mask in a Karl Süss MJB3 mask aligner for 20 - 25 s. at an intensity of 6 mW/cm<sup>2</sup> and a wavelength of 400 nm. Development is done in Shipley MF-319 developer for 25 s.

After development, metal is evaporated to create the connection pads and the alignment marks for the e-beam lithography. A 5 - 10 nm thick layer of chromium is first evaporated as a sticking layer followed by a 170 - 180 nm thick gold layer. Gold has a tendency to pick up organic contaminations which may cause problems with contacting the aluminum. A 5 - 10 nm thick

layer of Palladium is evaporated on top of the gold in order to prevent these problems. Lift-off is done in warm Remover 1165 or acetone depending on the layers beneath. When gold pads are fabricated on a multi layer chip the thickness of the gold layer is chosen so that the surface of the gold pads are matching the surface of the insulator.

### 5.3.2 Aluminium SQUID:s using E-beam lithography and shadow evaporation

E-beam resists 10 % Copolymer PMAA and ZEP520 diluted 1:2 in anisole thinner is used as bottom and top layers respectively. The resists are spun at 2000 rpm and at 1500 rpm giving thicknesses of 475 nm and 105 nm on a two inch wafer. For a 5 mm x 5 mm chip the resists are spun at 2500 rpm and 3000 rpm giving thicknesses of 400 nm and 100 nm. The resist layers are baked on hotplate at 135°C and 170°C for 5 min and 10 min respectively. The bottom layer has to be as thick as possible in order to get a smaller evaporation angle, preventing unwanted diffusion of aluminium during evaporation. Because the junction width is fairly large, 1.5  $\mu\text{m}$ , the top layer has to withstand the downward flex caused by its weight. Therefore the top layer is spun thick and baked at a high temperature in order to get a hard top layer.

Patterning is done using the JEOL JBX-3DII EBL system in MC2. Small structures were patterned with the fifth lens of the system at a current of 30 pA giving a spot size of 10 - 20 nm. Larger structures such as connection lines were patterned with the fourth lens at a current of 10 nA giving a spot size of 200 nm. The dose was adjusted according to the size of the features and proximity effect. A dose of 110  $\mu\text{C}/\text{cm}^2$  where used for silicon wafers and 125  $\mu\text{C}/\text{cm}^2$  for amorphous STO/SiO<sub>2-x</sub> multi-layers.

The top layer is developed for 45 s. in Oxylene and the bottom layer for 14 min in ECA:Ethanol 1:5. The chip is rinsed in IPA and blown dry after each development. The development time is extremely crucial for this device. There has to be an undercut of 150 nm minimum in order to get working SQUIDs. The undercut is visible in an optical microscope. The areas where the undercut is present are more transparent than the areas where it is absent.

After pumping down the evaporation system to  $1 - 2 \cdot 10^{-6}$  mbar, 35 nm of aluminium is evaporated at an angle of  $32^\circ$ . The surface of the aluminium is then oxidized at a partial pressure of  $8 \cdot 10^{-2}$  for 90 - 120 s. For junction sizes about  $1.5 \mu\text{m} \times 250 \text{ nm}$  this will give a resistance of 1 - 1.5 k $\Omega$ . Another 35 nm thick layer of aluminium is then deposited from the opposite angle,  $-32^\circ$ . Lift-off is done in warm Remover 1165 or acetone depending on the structures beneath.

## 5.4 Deposition of Capping and Insulation layer

All insulators were deposited at room temperature to prevent degradation of the YBCO and to be able to use a mask made by photolithography. Amorphous STO was deposited using Pulsed Laser Deposition and  $\text{SiO}_{2-x}$  using e-gun evaporation. Photolithography was used to form a mask. The processes described here was used to deposit insulating and capping layers between YBCO and aluminium on chip containing SQUIDs and on test chips for investigation of insulator's physical properties such as leakage currents and smoothness.

The process described in 5.3.1 was used to pattern the resist. When an insulating layer thicker than 200 nm is wanted, a lift-off layer consisting of several layers of LOL2000 is used. The first layer is spun and baked half of the stipulated time another layer is spun and baked half the stipulated time until the desired thickness is achieved. The last layer is baked the stipulated time, 5 min at 130 °C.

Silicon dioxide  $\text{SiO}_{2-x}$  is deposited using e-gun evaporation at a low rate 1 - 2 Å/s to prevent unnecessary heating of the chip. Pulsed laser deposition at room temperature is used to deposit amorphous STO, [30]. The process is described in section 5.1. Thousand, 1000 pulses at 0.9 mbar give a thickness of 225 - 250 nm.



# Chapter 6

## Measurement setup

Measurements have been performed at 4.2 K in liquid  $^4\text{He}$ , and at 300 mK with a pumped  $^3\text{He}$  cryostat. The general measurement setup is the same for both these cases, figure 6.1.

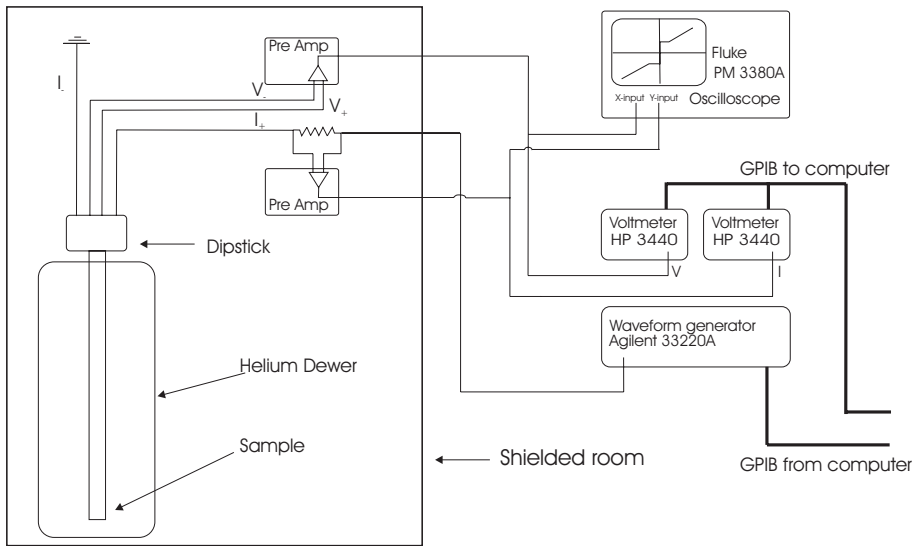


Figure 6.1: Schematic measurement setup. Standard four point measurements are performed in an electromagnetically shielded room. Battery driven preamplifiers amplify the output signal. The signals are measured by two voltmeters placed outside the shielded room. The voltmeters are connected via a GPIB interface to a computer.

The setup consists of: a dewer, a dipstick, battery driven preamplifiers, PAR 5113, inside the shielded room. Two voltmeters, HP 3440, an oscilloscope, Fluke 3380A, a waveform generator, Agilent 33220A, and a mea-

surement computer. The setup also consists of a temperature controller, Conductus LTC-20, which measures the temperature at the sample and a current source, Yokogawa 7651, coupled to a coil around the sample. All measurements lines are capacitively filtered and all lines in the dipstick are inductively filtered. It is possible to low pass filter the out-put signal.

All measurements have been performed using ordinary four point measurement in an electromagnetically shielded room. In the 4 K measurements the sample is placed on a long tube inside a vacuum jacket which is submersed in the dewer with liquid  $^4\text{He}$ . The 300 mK measurements have been performed with the Heliox VL system, which also is submersed into the dewer with liquid  $^4\text{He}$ . The sample is current biased by the waveform generator. The waveform generator is controlled by the computer via a GPIB interface. Current is measured by measuring the voltage over a resistor using a voltmeter. The voltage over the sample is measured by another voltmeter. The signal is amplified by the preamplifiers inside the shielded room. The voltmeters communicate with a computer which records the current and the voltage via a GPIB interface. The computer uses the LabView software. The outputs from the preamplifiers are also coupled to an oscilloscope. The oscilloscope enables the user to have quick preliminary results.

The setup has been used for measurements of I-V characteristics and the critical temperature. I-V characteristics of a device are obtained by ramping the current over the device using the waveform generator. A modulation of the output of the SQUIDs at a low magnetic field indicates that both junctions worked. The magnetic field was induced by a large coil inside the dipstick. In critical temperature measurements the sample is current biased by a fixed, fairly low, current. The voltage is measured and the Resistance - Temperature characteristic is obtained.

The aluminium structures are measured at 300 mK using the Heliox VL system from Oxford Instruments. The low temperature is obtained by pumping on  $^4\text{He}$  down to a temperature where  $^3\text{He}$  liquifies. By pumping on the liquefied  $^3\text{He}$  with a sorption pump a temperature of 265 - 290 mK is obtained. In principle the system works just as an ordinary fridge. Niobium screens were used in order to shield the sample from external magnetic field.

# Chapter 7

## Result and discussion

This chapter presents the results from the bottom of the chip to the top of the chip. It begins with the YBCO film and SQUIDs, continue with the insulating and surface properties of the capping and insulating layers and ends with the aluminium SQUIDs.

### 7.1 YBCO SQUIDs

The film was deposited as described in section 5.1 on  $0^\circ/30^\circ$  STO bi-crystal. The critical temperature  $T_c$  and the transition width of the film were determined by a susceptibility measurement. A critical temperature of 86.5 K and a transition width of 1 K were obtained. The crystallographic structure of the film was determined using X-ray diffraction, XRD. The spectra is presented in figure 7.1. YBCO has a tetragonal lattice structure and the  $c$ -axis lattice parameter is found by Bragg's law.

$$2d_{hkl} \sin \theta_{hkl} = n\lambda \quad (7.1)$$

The  $c$ -axis lattice parameter was found to be 11.68 Å. According to [35] and [36] this together with the critical temperature corresponds to a composition of 6.8 oxygen atoms per unit cell, i.e.  $YBa_2Cu_3O_{6.8}$ .

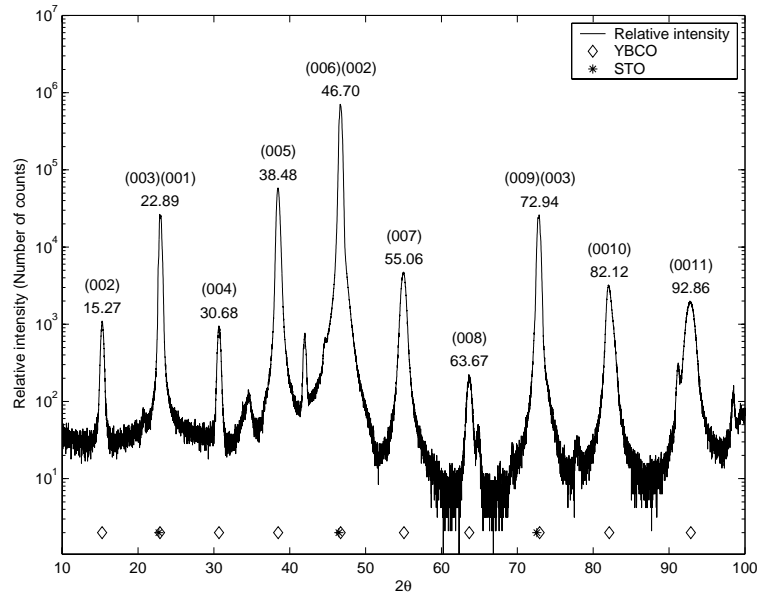


Figure 7.1: XRD spectra of the YBCO bi-crystal film used for SQUID fabrication. The peaks are labelled with their Miller indices, in the form (YBCO)(STO). The wavelength of the X-ray was  $1.54056 \text{ \AA}$ ,  $\text{CuK}\alpha_1$  and the angular resolution  $0.01^\circ$ .

The low critical temperature is known to be due to a bad YBCO source and probably contamination of the chamber. A test film made with the same settings and setup before the bi-crystal had a critical temperature of  $85.5 \text{ K}$ . Which may show that the heat up of the chamber during this deposition reduced the contamination of the chamber giving a better result for the second film.

The film was patterned using the standard recipe given in chapter 5. The electrical properties of the SQUIDs were determined by a standard four point dip-stick measurement in an unshielded environment.

The film is affected by the fabrication process. The width of the superconducting transition increased to  $2 \text{ K}$ . Unfortunately, reliable values of the critical temperature is hard to get though the thermometer has a limited accuracy and though it is not positioned close enough to the sample. However, the transition width should be reliable.

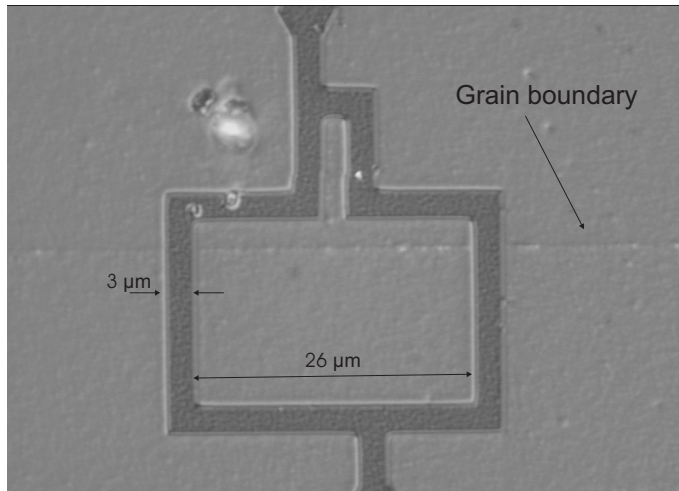


Figure 7.2: Image taken with optical microscope of a  $26 \mu\text{m} \times 18 \mu\text{m}$  large SQUID with  $3 \mu\text{m}$  wide grain boundary junctions. The  $0^\circ/30^\circ$  grain boundary is positioned in the middle of the SQUID, the line of defects. The grain boundary has a vertical misalignment of  $10 \mu\text{m}$ .

The I-V characteristics were measured for four SQUIDs. All SQUIDs had an area of  $18 \mu\text{m} \times 26 \mu\text{m}$  and a junction width of  $3 \mu\text{m}$ . Unfortunately, none of the  $15 \mu\text{m} \times 15 \mu\text{m}$  SQUIDs with junction width of  $1.5 \mu\text{m}$  worked. The open circuits are probably due to a large stitching error at top of the SQUID during the E-beam lithography and due to over etching. The critical and retrapping currents and the normal resistance were extracted from the data. The Stewart-McCumber parameter was determined by using equation 3.12. From  $\beta_c$  the SQUID capacitance is determined. The SQUID properties are summarized in table 7.1.

Table 7.1: Average and standard deviation of the Critical current,  $I_c$ , retrapping current,  $I_r$ , normal resistance,  $R_n$ , capacitance,  $C$ , and the Stewart-McCumber parameter,  $\beta_c$  for YBCO grain boundary SQUIDs measured at  $4.2 \text{ K}$ .

	Mean	Standard dev.
$I_c$ [mA]	1.31	0.066
$I_r$ [mA]	1.17	0.032
$R_n$ [ $\Omega$ ]	1.57	0.015
$C$ [fF]	122	8.3
$\beta_c$	1.24	0.11

The SQUIDs are slightly under-damped,  $\beta_c = 1.24$ . The deviations in

result between the SQUIDs are fairly small. The  $I_c R_n$  product equals 2.06 mV and the  $R_n C$  product 0.2 ps.

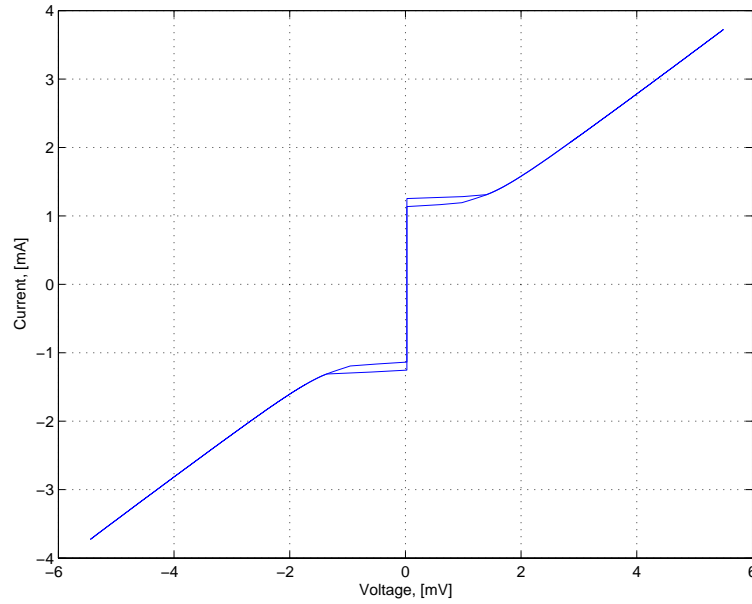


Figure 7.3: I-V characteristics of YBCO SQUID at 4.2 K. The SQUID have  $3 \mu\text{m}$  wide junctions on a  $0^\circ/30^\circ$  STO bi-crystal.

Because the SQUIDs were measured in an unshielded environment the devices may very well have trapped flux during the cool down and only a small modulation was observed for small magnetic fields. Flux trapped in the loop affects properties of the SQUIDs. The critical current may decrease due to the flux trapping, giving a lower value than what should be obtained without trapped flux in the loop. However, the SQUIDs would eventually produce a circulating current of  $650 \mu\text{A}$ . With a mutual inductance of 28 pH between the aluminium SQUID and the YBCO SQUID this current would couple an induced flux of the order of  $9\Phi_0$  to the surrounding aluminium SQUID.

## 7.2 Insulating properties of $\text{SiO}_{2-x}$

The experiment is described in section 4.5.1 and the fabrication in chapter 5. Figure 7.4 shows the lower left corner of the chip. The horizontal 260 nm thick YBCO stripes at the bottom are separated from the 62 nm thick vertical aluminium stripes by an intermediate 550 nm thick layer of thermally evaporated  $\text{SiO}_{2-x}$ . The nominal size of the YBCO/ $\text{SiO}_{2-x}$ /Al junctions in the image ranges between  $30 \mu\text{m}^2$  and  $130 \mu\text{m}^2$ .

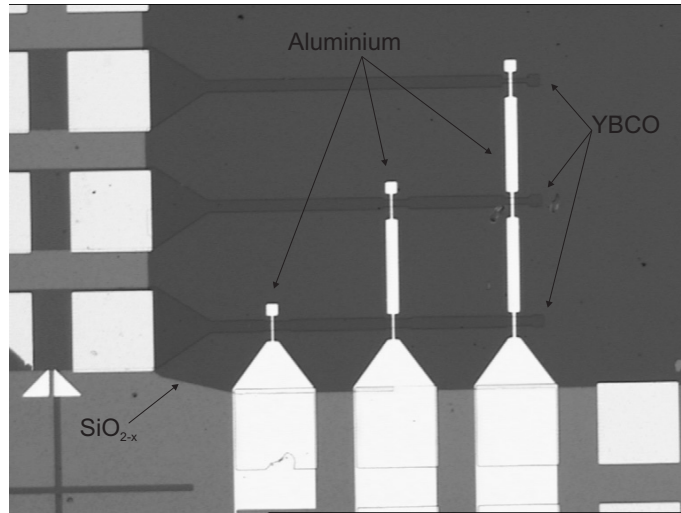


Figure 7.4: Lower left corner of chip used for studies of the resistance of  $\text{SiO}_{2-x}$ . Horizontal YBCO stripes in the bottom are separated from the vertical aluminium strips by a 550 nm thick intermediate layer of  $\text{SiO}_{2-x}$ . The size of the YBCO/ $\text{SiO}_{2-x}$ /Al junctions ranges between 30 and  $130 \mu\text{m}^2$ .

The I-V characteristics were determined at a temperature of 4.2 K for 6 of the 24 junctions at the chip. The nominal size of the junctions measured were, 20, 70, 90, 100, 130 and  $140 \mu\text{m}^2$ . Only six junctions were measured properly because of contact problems between the aluminium stripes and the gold pads caused by the lateral displacement of 400 nm between the pads and the Aluminium layer.

The approximative prediction, equation 3.28, corresponds well with the received I-V characteristics. The Schottky diode behavior of the junction appears clearly for temperatures below 100 K, and is reinforced as the temperature drops down to base temperature, 4-5 K. Resistance Voltage, R-V characteristics of the junctions were found by numerical differentiation of

the I-V characteristics. Results were obtained after compensation for the "network" effects associated with the design were done, figure 7.5.

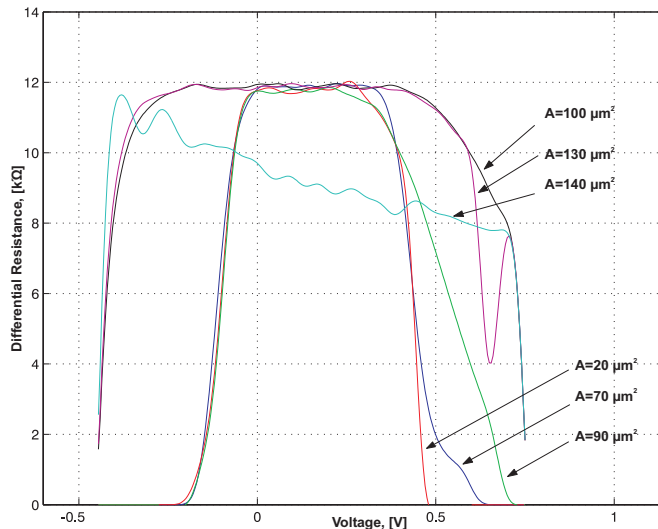


Figure 7.5: Resistance Voltage characteristics of YBCO/SiO<sub>2-x</sub>/Aluminium junctions at 4.2 K. The 260 nm thick bottom YBCO layer is separated from the 62 nm thick aluminium layer by an 550 nm thick intermediate layer of SiO<sub>2-x</sub>. The nominal area of the studied junctions are 20, 70, 90, 100, 130 and 140  $\mu\text{m}^2$ .

The resistance of the junctions studied is 12 k $\Omega$  in a 0.4 V range. The width of the resistive range tends to increase with the area of the junction. And the magnitude of the resistance seems to be independent of the junction area. The result contradicts the theoretical model presented in section 3.4. Further more, there are reasons to believe that the nominal areas of the junctions and the effective areas does not correspond to each other. The difference between the 90  $\mu\text{m}^2$  junction and the 100  $\mu\text{m}^2$  junction is small, but the width of the resistive range differs significantly. The argument is valid for the 20  $\mu\text{m}^2$  junction and the 70  $\mu\text{m}^2$  as well. Here, there is no difference in width, but a large difference in area. The results can be explained by considering the resistance to depend on the length of the weakest part of the structure. The width of the aluminium stripe was the same for the junctions with areas 20 - 90  $\mu\text{m}^2$  as well as for the junctions with areas 100 - 130  $\mu\text{m}^2$  and they show the same area dependence.

A similar experiment was performed for a barrier of amorphous STO, 240 nm and SiO<sub>2-x</sub>, 360 nm. The resistance of the barrier was found to be 9

k $\Omega$ . Thus every nanometer of SiO<sub>2-x</sub> seem to increase the resistance by 25  $\Omega$ .

A higher resistance was expected, [37]. The rather low resistance is most likely due to bad film quality. The quality of the film has not been investigated in more detail. Here a leakage current of 10 nA corresponds to a voltage difference of 120  $\mu$ V. This is too low if one wants to control the two SQUIDs individually as described in chapter 4. If it is impossible to increase the resistance of the SiO<sub>2-x</sub> film another more suitable insulator or another technique has to be chosen for the experiment.

### 7.3 Surface morphology and adhesion of capping/insulating layer

The surface morphology of thermally evaporated SiO<sub>2-x</sub> on top of STO, STO/amorphous-STO, STO/YBCO and STO/YBCO/amorphous-STO were investigated in Atomic Force Microscope. The morphology was compared by considering the peak-to-valley distance, P.to.V., i.e. the vertical distance between a valley and its neighboring peak. A 1  $\mu$ m x 1  $\mu$ m large scan and a surface profile of a SiO<sub>2-x</sub> surface thermally evaporated on top of STO are presented in figure 7.6.

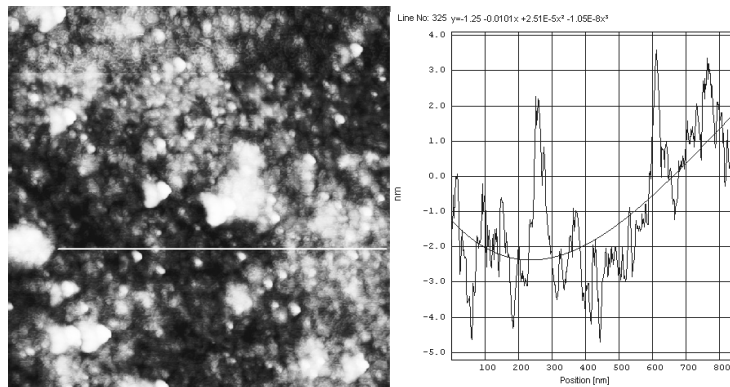


Figure 7.6: Left: AFM picture of a SiO<sub>2</sub> surface. The size of the scan was 1  $\mu$ m x 1  $\mu$ m and the scanned region was randomly chosen. The RMS roughness of the 1  $\mu$ m x 1  $\mu$ m scan was found to be 2.33 nm and the maximum peak to valley distance 4 - 5 nm. Right: Surface profile. The profile is indicated by the white line in the left figure.

The maximum P.to.V. distance for thermal evaporated SiO<sub>2-x</sub> on a bilayer of STO and amorphous STO is approximately 10 nm. For SiO<sub>2-x</sub> on

top of STO it is 4 - 5 nm. The layer of amorphous STO has a P.to.V. distance of approximately 15 nm and is making the  $\text{SiO}_{2-x}$  surface rougher. However, a thick layer of  $\text{SiO}_{2-x}$  seems to compensate the roughness of the amorphous STO.

$\text{SiO}_{2-x}$  on YBCO has a maximum P.to.V. distance of 10 nm. The P.to.V. distance of thermal evaporated  $\text{SiO}_{2-x}$  on top of YBCO and amorphous STO also equals 10 nm. Thus the amorphous STO does not contribute to any increase or decrease of the surface roughness. The P.to.V. distance did not change for aluminium deposited on top of the  $\text{SiO}_{2-x}$ .

The P.to.V. distance for a Silicon wafer with a  $0.44 \mu\text{m}$  thick layer of  $\text{SiO}_2$  is approximately 4 - 5 Å and less than 1 nm for a STO chip. This is less than one tenths of the P.to.V. distance for thermal evaporated  $\text{SiO}_{2-x}$  on amorphous STO on a STO chip. The roughness of the film may be a problem for post processing. The amorphous STO, deposited under the conditions given in section 5.4, appears to cause the largest surface roughness. A smoother capping layer is desirable.

Problems with adhesion of the  $\text{SiO}_{2-x}$  have arised during the experiments. In figure 7.7 three examples of bad adhesion of  $\text{SiO}_{2-x}$  are presented.

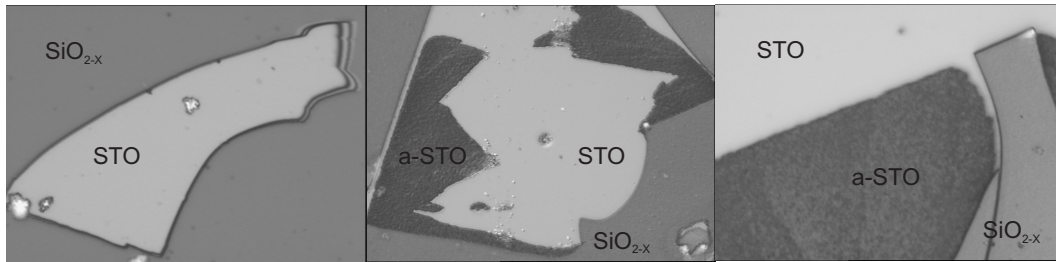


Figure 7.7: Left: Optical micrograph of a  $60 \mu\text{m}$  wide hole in the  $\text{SiO}_{2-x}$  layer from the chip used for resistance measurements. Middle and Right: Region where the  $\text{SiO}_{2-x}$  layer has come loose but not all of the underlying layer of amorphous STO.

The images show that  $\text{SiO}_{2-x}$  film had a tendency to come loose adjacent to cracks in the film. The cracks are caused by heating of the chip when baking e-beam resist. The images also show that the amorphous STO seems to stick better than the  $\text{SiO}_{2-x}$ . The cracks in the  $\text{SiO}_{2-x}$  are most likely due to differences of the thermal expansion coefficients,  $\alpha$ , for the  $\text{SiO}_{2-x}$ , the YBCO film and the STO. Thermal expansion coefficient for  $\text{SiO}_{2-x}$  is

$\alpha = 0.6 - 0.9 \cdot 10^{-6} \text{ K}^{-1}$  and for YBCO and STO  $\alpha \simeq 1 \cdot 10^{-5} \text{ K}^{-1}$ , [38]. This argument may also explain why the amorphous STO sticks better.

The process has to be adjusted so that heating temperatures and times of the samples are reduced. Having a lower background pressure during the deposition of the film may also increase the adhesion of the  $\text{SiO}_{2-x}$  to the underlying layers. A thinner film may cope better with the thermal strain.

## 7.4 YBCO degradation

Degradation of the superconducting properties of YBCO has been studied in two experiments. The impact on the film quality due to deposition of a two material capping and insulating layer on top of a bare film and processing on top of this multi-layer is discussed first. The second experiment studies how the critical current of a grain boundary junction is affected by the capping/insulating layers.

A 120 nm thick layer of amorphous STO was deposited on top of the YBCO film at room temperature. A 500 nm thick layer of  $\text{SiO}_{2-x}$  was thermally evaporated on top of the amorphous STO. Goldpads and alignment marks were fabricated at the chip using the procedure presented in section 5.3.1. E-beam lithography for aluminium SQUIDs and shadow evaporation together with lift-off was performed three times. For details see section 5.3.2. Baking of resist involved heating the chip up to 170 ° C for 10 min three times, to 135 ° C for 5 min four times and up to 110 ° C one time. Further more, the chip was ion milled for 31 min at an accelerating voltage of 400 V and a current of 0.1 mA.

The film had a critical temperature,  $T_c$  of 85.5 K and transition width,  $\Delta T_c$  of 1 K after being deposited. The post processing critical temperature was lowered 1.5 K to 84 K, and the transition width increased to 5 K.

The decrease of  $T_c$  and the increase of  $\Delta T_c$  is thought to be due out-diffusion of oxygen from the YBCO film. The increase in  $\Delta T_c$  show that some parts of the film are more exposed than other. Such parts may very well be the corners and the borders of the film or other parts that are not well protected. The amorphous STO may extract oxygen from the YBCO. The  $\text{SiO}_{2-x}$  may act the same way on the film. However, there are reasons to believe that heating the chip up to 170 ° C several times caused the largest damage.

The SQUIDs discussed in section 7.1 were characterized at 4.2 K after deposition of a capping and insulating layer on top of them. A 240 nm thick layer of amorphous STO was deposited using PLD at room temperature and a 360 nm thick layer of  $\text{SiO}_{2-x}$  was thermally evaporated on top of the SQUIDs. The critical temperature decreased 1 K and the transmission width increased 1 K, to 4 K, due to the post processing. Average values of the critical current, the retrapping current, the normal resistance, the SQUID capacitance and the damping parameter are presented in table 7.2. For comparison the average values for the same SQUIDs prior to the insulation/capping process are presented in the rightmost column.

*Table 7.2: Average and standard deviation of the Critical current  $I_c$ , retrapping current  $I_r$ , normal resistance  $R_n$ , capacitance,  $C$ , and the Stewart-McCumber parameter  $\beta_c$  for YBCO grain boundary SQUIDs after deposition of a-STO and  $\text{SiO}_{2-x}$  at 4.2 K. In the rightmost column the average values from the measurement with uncapped junctions are presented.*

	Mean, capped	Standard dev.	Mean, uncapped
$I_c$ [mA]	1.73	0.26	1.31
$I_r$ [mA]	1.56	0.22	1.17
$R_n$ [ $\Omega$ ]	1.32	0.08	1.57
$C$ [fF]	128	3.53	122
$\beta_c$	1.19	0.06	1.24

The increase in critical current and retrapping current are most probably due to less flux trapping in the film, [16]. If the films are of poor quality there are a lot of defects that may trap flux and affect the properties of the junctions. However, the increase of  $I_c$  and  $I_r$  shows that the layer of amorphous STO and  $\text{SiO}_{2-x}$  has not damaged the junctions significantly. The capacitance has not changed considerably and the  $I_c R_n$  product still equals approximately 2 mV. The dynamic properties of the SQUIDs,  $\beta_c$ , has not changed either. The proposed materials in the capping/insulating layer seem to be good choices if the properties of the junctions are considered even though the critical temperature of the YBCO decreased.

## 7.5 Aluminium SQUIDS

Aluminium SQUIDS were fabricated on silicon chips using electron beam lithography and shadow evaporation to develop the technology. Process parameters were determined from the experiments. For details regarding the fabrication, see section 5.3.2. The SQUIDS were characterized below 300 mK in an electromagnetically shielded environment. Attempts to fabricate aluminium SQUIDS on top of a STO/YBCO/a-STO/SiO<sub>2-x</sub> multi-layer were done.

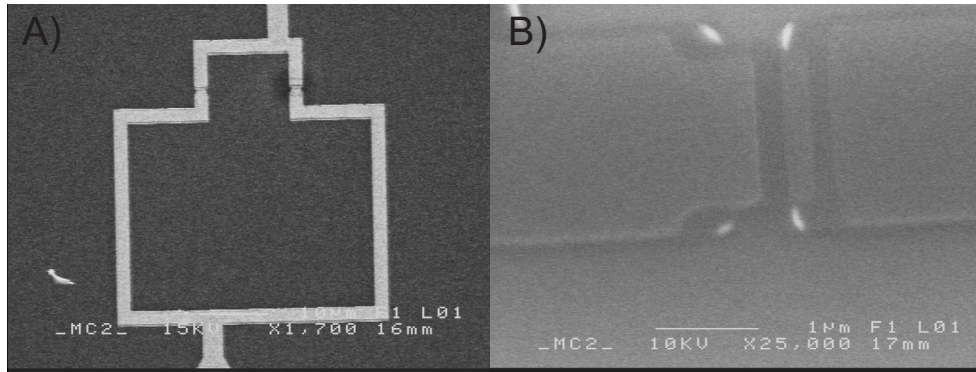


Figure 7.8: Scanning electron microscope image of a aluminium SQUID and a junction. Left: Aluminium SQUID with area  $28 \mu\text{m} \times 36 \mu\text{m}$  and  $1.5 \mu\text{m}$  wide junctions. Right: A  $1.5 \mu\text{m}$  wide and  $250 \text{ nm}$  deep aluminium junction.

The critical temperatures of the samples that were measured were in the range  $1.4 - 1.6 \text{ K}$ . The superconducting energy gap was found to be  $0.2 \text{ meV} - 0.22 \text{ meV}$ . The results correspond well with BCS theory for weak coupling. In table 7.3 average values of the critical current,  $I_c$ , retrapping current,  $I_r$ , normal resistance,  $R_n$ , and the Stewart-McCumber parameter,  $\beta_c$ , for aluminium SQUIDS with different junction size are presented. The junction width of the measured SQUIDS were  $0.5, 0.7, 1.0$  and  $1.5 \mu\text{m}$ .

Table 7.3. Average values of the critical current,  $I_c$ , retrapping current,  $I_r$ , normal resistance,  $R_n$ , and the Stewart-McCumber parameter,  $\beta_c$ , for aluminium SQUIDs with different junction size. The aluminium had a critical temperature of 1.58 K and the superconducting gap was 0.22 meV. The SQUIDs were measured below 288 mK.

$w_{junc}$ [ $\mu\text{m}$ ]	$d_{junc}$ [nm]	$I_c$ [nA]	$I_r$ [nA]	$R_n$ [k $\Omega$ ]	$\beta_c$
0.5	250	8.5	0.9	4.39	190
0.7	250	9.8	1.2	4.05	160
1.0	250	36	5.3	1.86	350
1.5	250	56	8.8	1.29	310

The Stewart-McCumber parameter is calculated using the formula presented in equation 3.12. The results imply that the SQUIDs are under damped. The SQUIDs have an average capacitance of 0.8 pF/ $\mu\text{m}^2$ , which is of the same order as reported in [32]. The average  $R_n A$  product is 980  $\Omega\mu\text{m}^2$ .

The  $I_c R_n$  product for the SQUIDs with the two largest junctions, 1  $\mu\text{m}$  and 1.5  $\mu\text{m}$ , equals 0.069 mV and 0.072 mV. The results deviate a factor five from what one get with the Ambegaokar-Baratoff formula, equation 4.1, at 300 mK, 0.34 mV. The deviations may be caused by a high noise temperature due to noise in the system. This discrepancy indicates a noise temperature of 6 K, which should be compared with the 1.55 K in [15].

The experiment showed that the design most suitable for qubit readout is the one with the largest junction size, 1.5  $\mu\text{m}$  x 250 nm. This design has the highest critical current and the highest  $I_c R_n$  product. The higher critical current enables more precise readout and the higher  $I_c R_n$  product implies that they have a higher quality. It should be mentioned that this design also has the highest reproducibility. However, the critical current is not as high as reported in [11] and [15], 109 nA and 400 nA respectively.

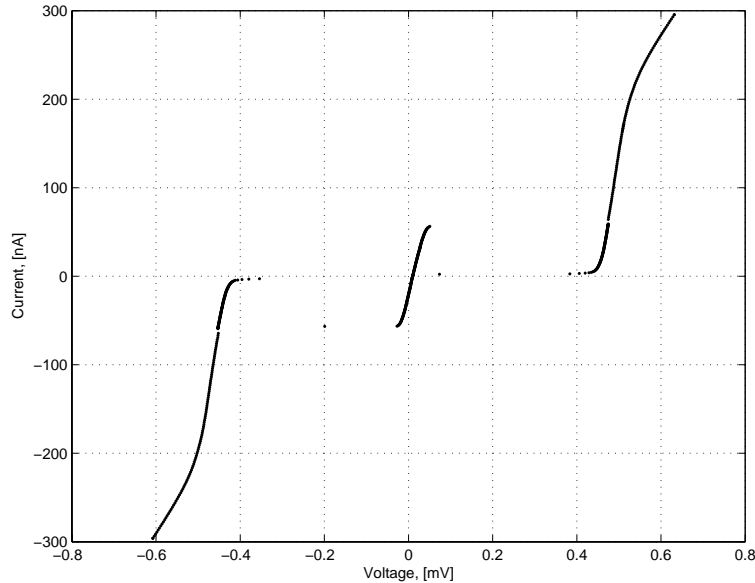


Figure 7.9: I-V characteristics of a SQUID with  $1.5 \mu\text{m}$  wide junctions at 288 mK. The SQUID have critical current,  $I_c$  of 56 nA, a retrapping current of 4.5 nA and a normal resistance of 1.29 k $\Omega$ . The critical temperature of the film was 1.58 K and the superconducting gap 0.22 meV. The leaning behavior of the S-branch is due to a resistance in series with the SQUID.

Attempts to fabricate aluminium SQUIDs on top of a STO/YBCO/a-STO/SiO<sub>2-x</sub> multi-layer were done. This configuration is very similar to the configuration proposed in chapter 4. As mentioned in section 7.4 the peak-to-valley distance for this surface is a factor ten larger than for a silicon surface. It is also much harder to get good uniformity of a thick resist layer on a 5 mm x 5 mm chip than on a two inch wafer. The procedure presented in section 5.3.2 and 5.3.1 were used when fabricating the samples. An image of a  $18 \mu\text{m} \times 18 \mu\text{m}$  large SQUID with  $1.5 \mu\text{m}$  wide junctions fabricated on this surface taken with an optical microscope is presented in figure 7.10.

In order to get the desired undercut and resolution the dose during the E-beam lithography was increased to 125  $\mu\text{C}/\text{cm}^2$ . After development the pattern showed no major differences between this setup and the silicon chip setup. However, problems arose during the lift-off of the aluminium. Lift-off was done in warm acetone or warm remover 1165. The aluminium did not stick to the surface on some parts of the chip, mostly the connection lines.

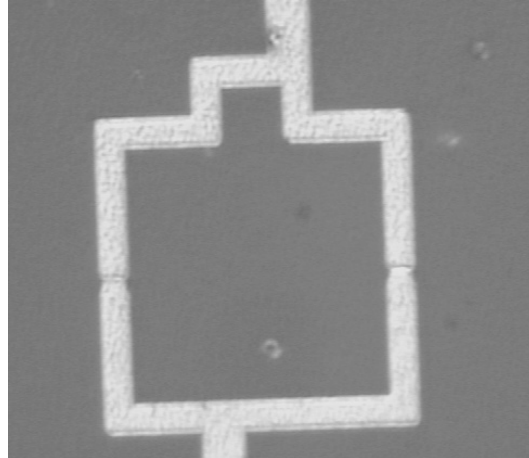


Figure 7.10: Image taken with an optical microscope of a  $18\ \mu\text{m} \times 18\ \mu\text{m}$  large aluminium junction fabricated on a layer thermal evaporated  $\text{SiO}_{2-x}$ .

The bad adhesion may have several reasons. An insufficient undercut making the aluminium in the developed parts and the undeveloped parts fused together. When doing lift-off the metal that should be removed may pull away metal in the developed parts of the pattern if the sticking to the surface is too weak. This problem is enhanced when doing shadow evaporation with relatively large angles. Another reason may be bad adhesion. That the aluminium does not stick to the surface or that the surface material does not stick to itself. However, the problem has not been examined carefully enough to draw any conclusions.

Despite this unsuccessful experiment one conclusion could be made. The process needs more testing. As shown in figure 7.10 the geometry of the SQUID is the desired one and the SQUIDS work on silicon chips. If process parameters for this setup are determined aluminium SQUIDS could be tested as readout devices for flux-qubits in multi-layer structures.

# Chapter 8

## Conclusion

We have proposed and investigated the feasibility on HTS flux qubit read-out device using low- $T_c$  aluminium SQUIDs. The proposed device consists of a grain boundary YBCO SQUID and a surrounding aluminium SQUID separated by an intermediate insulating and capping layer. Each part of the device has been studied within this project.

YBCO SQUIDs with  $0^\circ/30^\circ$  grain boundary Josephson junctions have been fabricated using electron beam lithography and ion milling through an amorphous carbon mask. The junctions of the SQUIDs were  $3 \mu\text{m}$  wide and the area of the SQUIDs  $470 \mu\text{m}^2$ . The SQUIDs were characterized at 4.2 K in a magnetically unshielded environment and showed a slightly under-damped behavior,  $\beta_c = 1.24$ . The critical current of a typical SQUID was found to be 1.5 mA and the normal resistance  $1.45 \Omega$ . However, the deviations between different measurements were large, probably due to trapping of flux in the SQUIDs. Critical currents from 1.3 mA to 2.1 mA were obtained.

Resistance - Voltage characteristics have been determined for YBCO/ $\text{SiO}_{2-x}$ /aluminium junctions of various sizes at 4.2 K. A 550 nm thick intermediate layer of thermally evaporated  $\text{SiO}_{2-x}$  showed a resistance of  $12 \text{ k}\Omega$  in a 400 mV wide range around zero. A barrier consisting of a 240 nm thick layer of amorphous STO and 360 nm thick layer of  $\text{SiO}_{2-x}$  had a resistance of  $9 \text{ k}\Omega$ . The resistance of the intermediate layer is lower than expected and do need to be increased a factor ten to get this device to work properly. Improvements of the film quality has to be done or a different insulator or technique has to be chosen for the device.

The surface roughness of thermally evaporated  $\text{SiO}_{2-x}$  on top of a layer of amorphous STO on a STO chip is ten times larger than the roughness of a

STO chip and twenty times larger than the roughness of a silicon wafer with a buffer layer of  $\text{SiO}_2$ . The peak-to-valley distance was found to be approximately 10 nm for thermally evaporated  $\text{SiO}_{2-x}$  on top of a layer of amorphous STO on a STO chip. The peak-to-valley distance for the amorphous STO was 15 nm. The roughness of the  $\text{SiO}_{2-x}$  was not affected if a layer of YBCO was present under the amorphous STO or not. A thin layer of aluminium on top of the  $\text{SiO}_{2-x}$  neither increased or decreased the roughness of the surface.

Deviations in the thermal expansion coefficients of  $\text{SiO}_{2-x}$  and STO, YBCO caused cracks in the  $\text{SiO}_{2-x}$  film when the sample was heated during processing. The stress caused by the unmatched thermal expansion is one reason for the sometimes bad adhesion of  $\text{SiO}_{2-x}$  to STO or amorphous STO.

It was found that a multi layer of amorphous STO, deposited at room temperature, and thermally evaporated  $\text{SiO}_{2-x}$  on top of YBCO grain boundary SQUIDs did not change the properties of the  $0^\circ/30^\circ$  grain boundary Josephson junctions. It was also found that post processing on the surface of the multilayer caused a lowering of the critical temperature and an increase of the transition width of the YBCO if the chip was heated up to  $170^\circ$  during the processing. Thus the tested multi-layer do not degrade the properties of the junctions. However, high temperatures during processing may be destructive for the film despite the capping layer.

Aluminium SQUIDs have been fabricated on silicon chips using electron beam lithography and shadow evaporation. Josephson junctions of various size have been tested. The aluminium SQUIDs have been characterized below 300 mK. The maximum critical current was obtained for the SQUIDs with junction width of  $1.5 \mu\text{m}$ ,  $I_c = 56 \text{ nA}$ . These SQUIDs showed the highest reproducibility and had a normal resistance of  $1.3 \text{ k}\Omega$ . The  $I_c R_n$  product equaled  $0.072 \text{ mV}$ , which is a factor five less than predicted. This deviation gives an estimate of the noise temperature of the SQUIDs, 6 K. Attempts to fabricate Aluminum SQUIDs using the same techniques on top of STO/YBCO/amorphous-STO/ $\text{SiO}_{2-x}$  have been done. Non of these attempts resulted in working SQUIDs due to problems with lift-off.

All parts of the proposed device have been studied and investigated. The aluminium SQUIDs were found to work on silicon chips and the YBCO SQUIDs were found to work on STO substrates, with or without capping, respectively. However, the insulation of the intermediate layer has to be increased, at least a factor ten. The adhesion for metals deposited on top of the intermediate layer also has to be improved and the roughness of the capping

and insulating layer may very well need to be reduced. The key issue for this project is thus to improve the performance of the intermediate layer, even if this not is a problem for a qubit device because it would not have any leads and thus would not need any insulation. New materials with more suitable properties or new techniques such as air bridges may be the solution. If the problems with the intermediate layer are solved more knowledge about the feasibility of using aluminium SQUIDs for HTS flux qubit read-out could be gained.

The project had 14 targets, see section 2.1. 12 - 13 of these targets have been fulfilled. Though the master thesis is the last part of 4.5 years of education it is relevant to mention the skills and competencies I have develop during the project. I have structured the work and I have introduced the general idea of the project myself. I have designed the devices to fit the requirements and I have got knowledge about the dynamics of Josephson junctions in LTS and HTS materials and material properties of amorphous insulators. During this twenty weeks I have learnt to; perform electron beam lithography, deposit metals and insulators using different deposition techniques, get images of aluminium structures on silicon by using a scanning electron microscope, perform ion etching on YBCO and metals, do photolithography and perform characterization of devices down to 4.2 K. I have got an introduction to; epitaxial film deposition using PLD, atomic force microscopy and cryogenics down to 265 mK. This report together with a lot of experience summarize the project.



# Bibliography

- [1] S. Lloyd, *Ultimate physical limits to Computation*, Nature, vol **406**, pp 1047-1054, (2000).
- [2] M. A. Nielsen, I. L. Chuang *Quantum Computation and Quantum Information*, Cambridge University Press, 2001.
- [3] I. L. Chuang, N. Gershenfeld, M. Kubinec, *Experimental Implementaion of Fast Quantum Searching*, Phys. Rev. Lett., vol **80**, pp 3408-3411, (1998).
- [4] L. M. K. Vandersypen, M. Steffen, G. Breyta, C. S. Yannoki, M. H. Sherwood, I. L. Chuang, *Experimental realization of Shor's quantum factoring algorithm using nuclear magnetic resonance*, Nature, vol. **414**, pp 883-887, (2001).
- [5] , S. Guide, M. Riebe, G. P. T. Lancaster, C. Becher, J. Eschner, H. Haffner, F. Schmidt-Kaler, I. L. Chuang, R. Blatt, *Implementation of the Deutsch-Jozsa algorithm on an ion-trap quantum computer*, Nature, vol **421**, pp 48-50, (2003)
- [6] G. Wendin, *Superconducting quantum computer*, Physics World, May 2003, pp 3-4, (2003).
- [7] Y. Nakamura, Yu. A. Pashkin, J. S. Tsai, *Coherent Control of macross-copic quantum states in a singel-Cooper-pair box*, Nature, vol. **398**, pp 786-788, (1999).
- [8] J. E. Mooij, T. P. Orlando, L. Levitov, L. Tian, C. H. van der Wal, S. Lloyd, *Josephson Persistent-Current Qubit* , Science, vol **285**, pp 1036-1039, (1999).
- [9] J. Freidman, V. Patel, W. Chen, S. Tolpygo, J. Lukens, *Quantum superposition of distinct macroscopic states* , Nature, vol **406**, pp 43-46, (2000).

- [10] C. H. van der Wal, A. C. J. ter Haar, F. K. Wilhelm R. N. Schouten, C. J. P. M. Harmans, T. P. Orlando, S. Lloyd, J. E. Mooij, *Quantum Superposition of Macroscopic Persistent-Current States*, Science, vol **290**, pp 773-777, (2000).
- [11] Caspar van der Wal, *Quantum Superpositions of Persistent Josephson currents*, Technische Universiteit Delft, Netherlands, 2001.
- [12] M. H. S. Amin, A. Yu. Smirnov, A. M. Zagoskin, T. Lindström, S. Charlebois, T. Claeson, A. Ya. Tzalenchuck, *Silent Phase Qubit based on d-Wave Josephson Junctions*, Submitted to Applied Physics Letters, 22/09/2003.
- [13] A. Ya. Tzalenchuck, T. Lindström, S. A. Charlebois, E. A. Stepantsov, A. M. Zagoskin, Z. Ivanov, T. Claeson, *Feasibility Studies of Ultra-Small Josephson Junctions for Qubits*, IEEE Transactions on Applied Superconductivity 13:948-951 (2003).
- [14] T. Lindström, S. A. Charlebois, A. Ya. Tzalenchuck, Z. Ivanov, M. H. S. Amin, A. M. Zagoskin, *Dynamical Effects of an Unconventional Current-Phase Relation in YBCO dc SQUIDS*, Phys. Rev. Lett., vol **90**, 117002, (2003).
- [15] H. Tanaka, Y. Sekine, S. Saito, H. Takayanagi, *DC-SQUID readout for qubit*, Physica C, vol **368**, pp 300-304, (2002).
- [16] J. R. Waldram, *Superconductivity of Metals and Cuprates*, IOP Publishing Ltd, 1996.
- [17] R. P. Feynman, *The Feynman Lectures on physics, Vol. III, Quantum Mechanics*, Addison-Wesley Publishing Company, 1971.
- [18] K. K. Likharev, *Dynamics of Josephson Junctions and circuits*, 2:nd edition, Gordon and Breach Science Publishers, 1991.
- [19] E. Il'ichev, V. Zakosarenko, R. P. J. Ijsselsteijn, H. E. Hoening, V. Schultze, H. Meyer, M. Grajcar and RHLubina, *Anomalous periodicity of the current-phase relationship of grain-boundary Josephson junctions in high- $T_c$  superconductors*, Physical Review B, vol **60**, pp 3096-3099, (1999).
- [20] W. C. Stewart,, Appl. Phys. Lett., vol **12**, pp 277, (1968).
- [21] D. E. McCumber,, J. Appl. Phys., vol **39**, pp 3113, (1968).

- [22] H. H. Zappe, *Minimum current and related topics in Josephson tunnel junction devices*, Journal of Appl. Phys., vol **44**, pp 1371-1377, (1973).
- [23] E. J. Tarte, G. Wagner, R. Somekh, F. Baudenbacher, P. Berghuis, J. Evetts, *The Capacitance of bicrystal Josephson junctions Deposited on SrTiO<sub>3</sub> substrates*, IEEE Transactions on Applied Superconductivity, vol **7**, pp 3662-3665, (1997).
- [24] M. Tinkham, *Introduction to superconductivity*, McGraw-Hill, 2:nd edition, 1996.
- [25] G. Brorsson, E. Olsson, P. Nilsson, T. Claeson, *Growth and properties of YBa<sub>2</sub>Cu<sub>3</sub>O<sub>7-x</sub>/(SrTiO<sub>3</sub>/PrGaO<sub>3</sub>)/YBa<sub>2</sub>Cu<sub>3</sub>O<sub>7-x</sub> trilayers: Optimization of the insulation*, J. Appl. Phys., vol **75**, pp 827-834, (1994).
- [26] J. D. Suh, G. Y. Sung, S. G. Lee, D. K. Kim, *High quality YBCO/STO Bilayers for superconducting Electric Field Effect Transistor*, Physica C, vol **282-287**, pp 695-696, (1997).
- [27] S. Tokunaga, Y. Ohkawa, K. Suzuki, Y. Enomoto, *SiO<sub>2</sub> passivation film effects on YBCO junctions*, Physica C, vol **306**, pp 107-113, (1998).
- [28] Q. X. Jia, W. A. Anderson, *SiO<sub>2</sub> and Si<sub>3</sub>N<sub>4</sub> passivation layers on YBCO thin films*, J. Appl. Phys., vol **66**, pp 452-454, (1989).
- [29] W. Kula, W. Xiong, R. Sobolewski, *Laser Patterning of YBCO thin films protected by in-situ grown STO cap layer*, IEEE Transactions on Applied superconductivity, vol **5**, pp 1177-1180, (2000).
- [30] T. J. Hwang, D. H. Kim, K. W. Lee, Y. K. Park, *Fabrication of YBCO/STO/YBCO multilayer by PLD*, Physica C, vol **341-348**, pp 2347-2348, (2000).
- [31] D. A. Neamen, *Semiconductor Physics and Devices: basic principles*, 2:nd edition, Irwin/McGraw-Hill, 1997.
- [32] K. Bladh, *The Single Cooper Pair Box - Read out by a Radio Frequency Singel Electron Tranistor*, Chalmers Univeristy of Technology, Göteborg, 2002.
- [33] I. Nkrumah, *Effect of Gallium Ions on Yttrium Barium Copper Oxide*, Chalmers Univeristy of Technology, Göteborg, (2003).
- [34] A. Tzalenchuck, S. Chalebois, T. Lindström, E. Stepantsov, Z. Ivanov, *Report on technology*, manuscript, (2002).

- [35] S. Rusiecki, B. Bucher, E. Kaldis, E. Jilek, J. Karpinski, C. Rossel, B. Pümpin, H. Keller, W. Kündig, T. Krekels, G. van Tendeloo, *123 Near equilibrium samples anomalies of the lattice parameters and some physical properties*, Journal of Less-Common Metals , vol **164 & 165**, pp 31-38, (1990).
- [36] A. W. Hewat, P. Fisher, E. Kaldis, E. A. Hewat, E. Jilek, J. Karpinski, S. Rusiecki, *Cu-O bond and  $T_c$  changes in 123, 124 & 247-superconductors*, Journal of Less-Common Metals , vol **164 & 165**, pp 39-49, (1990).
- [37] M. Ohring, *The Materials Science of Thin Films*, Academic Press, London, 1992.
- [38] M. Ban, K. Suzuki, Y. Enomoto,  *$SiO_2$  passivation film effects on microwave characteristics of  $Yb_{a_2}Cu_3O_{7-x}$ -based resonators* Journal of Appl. Phys., vol **290**, pp 345-353, (1997).